Master Thesis

Raman Gain Optimization in Multi-band Optical Transmission

Giacomo Borraccini

Supervised by
Vittorio Curri
Alessio Ferrari
Stefano Straullu

Final Project Report for the
Master in Electronic Engineering

Department of Electronics and Telecommunications, DET
Politecnico di Torino
Italy, Turin

October 2019

Raman Gain Optimization in Multi-band Optical Transmission

Giacomo Borraccini

Supervised by:

Vittorio Curri
DET
Alessio Ferrari
DET
Stefano Straullu
LINKS

Abstract

In optical transmissions, a fundamental role is covered by optical amplifiers, which allow to propagate the transmitted signal along the fiber link even for huge routes restoring the optical power level. Recently, the focus of the research - and also of the market - moves to the comprehension of the Raman effect and to its applications on the optical amplification.
Starting from a physical layer description of an optical fiber link, an optimization tool has been developed to make efficient and suitable the design of Raman amplifiers. The optimization framework is able to refine design parameters of Raman pumps - as input optical power and wavelength - to get the maximum performance in terms of gain profile. The investigation is centered on multi-band optical transmission scenarios.
After a general overview on the world of optical communication, considering mainly optical amplifiers characteristics and Raman effect basics, the present work treats and describes methodologies and algorithms on which the optimization tool is based, discussing cases under examination with the relative analysis. Then, results obtained during the research activity show that the developed framework can design Raman amplifiers with impressive performances.
The presented optimization structure is just an initial automatic tool for the design of Raman amplifiers in multi-band scenarios. In the further development, it can be refined and improved, enlarging the range of features to optimize and reducing the time of execution.

Acknowledgements

My first sincere thanks goes to Professor Vittorio Curri. In addition to the precious teachings, his enterprising spirit and intuition have been illuminating during the whole thesis activity. Thanks to his experience, I have observed how to manage the research cycle from the beginning and I have learnt how to critically analyze results in order to set the prosecution of the investigation.
I would like to warmly thank Alessio Ferrari to whom I owe my current vision of research and the largest part of technical teachings. I'll never forget all his answers to the infinite number of questions that I posed during these months.
Furthermore, I would like to thank the entire OptCom group for making me feel integral part of the team and for having shared intense moments of work and fun.

My greatest gratitude goes to my colleagues and friends Giorgio and Manfredi, with whom I grew up, passing exam by exam shoulder to shoulder. Even if our paths split, despite the distance, their advice and observations have been particularly helpful for the development of this work.
I would like to thank also my roommates Paolo and Marco, for their capability to cheer me up even in moments of difficulty and for the reciprocal help shown in this last period of thesis.
I am very grateful also to my colleagues Arian and Francesca and my dear friend Benedetta for their advice in terms of thesis layout and image adjustment.

I would also like to mention the huge support of all my colleagues and friends in Turin and Ascoli Piceno. In particular I want to thank Paolo and Lorenzo, fantastic musicians and adventure companions, for their time spent on me and for always having right words for me.

I would never have the possibility to present this work without my wonderful family. Despite the difficulties I met inside and outside University courses in these years, they were always there to encourage me and to make me believe that the road is downhill. A special thanks goes to my second family in Turin for the huge help that gave me, treating me like a son.

Contents

List of Figures

List of Tables

Chapter 1

Motivations and Goals

Observing the layout defined by the 5G road map and by the Internet of Things overflow, it is almost straightforward to identify what are the main centers of interest of the market and the direction of further business and technological improvement in telecommunications.
From a very general - but not trivial - point of view, it is possible to resume the main guidelines which move the scientific effort toward the development of advanced communication systems in two simple principles:

- **The improvement of the quality of the transmission**, targeted at obtaining a larger exchange of data among users, and so a faster communication;
- **The enlargement of the capability of communication systems**, aiming to manage an increasing number of users in a specific network.

Embracing these concepts, industrial vendors and researchers have set out a new prospective, establishing the basics for developing even more efficient, integrated and highly performing communication systems.
In particular, considering the field of optical communications, devices are taken under analysis investigating physical and technological aspects, trying to deduce more accurate models or to improve matters' properties. New techniques related to different systemic approaches are tested in order to take advantage in the transmission quality rate and more efficient software algorithms are exploited to manage the increasing amount of traffic data in the global network.

In optical transmissions, a fundamental role is covered by optical amplifiers, which allow to propagate the transmitted signal along the fiber link even for huge routes restoring the optical power level.
In the 90s and in the early 2000s, optical amplifiers were based on the exploitation of the fiber doping with Erbium, leading to the achievement of performance maximum of EDFAs (Erbium Doped Fiber Amplifiers).
Recently, the focus of the research - and also of the market - moves to the comprehension of the Raman effect ([10], [2], [18]) and to its applications on the optical amplification. The main reasons that bring to the use of this technique are related to the before mentioned principles:

- At the same gain level, Raman Amplifiers (RAs) allow to get a lower noise contribution with respect to EDFAs, enhancing the improvement of performances;

- Building up a proper design, the use of Raman amplification allows to extend the frequency spectrum for optical communications and to manage also a very dense input signals' pattern.

Following this direction, it has been also possible to design and to realize hybrid systems which exploit both Raman and Erbium doped fiber amplifications, able to achieve a significant trade-off joining high performances with multi-band optical transmissions.

The goals of the investigation are related to the analysis of the Raman amplification in likely practical scenarios and the subsequent development of a tool able to give the guidelines on the choice of input parameters for a certain amplifier design. In particular, the interest is focused on the design of the input power entity and wavelength of each Raman pump that forms the Raman amplifier and the evaluation of its performances though the modification of the system working point passing from single band condition (C band only) to multi-band condition (C+L bands).

The thesis is articulated into three main parts.
The first one makes reference to Chapter 2 - Introduction on Optical Communication Systems - and it is an preface on the fundamentals for the comprehension of optical communications, operating a successive digression on optical amplifiers and Raman effect in terms of applications and physical characterization.
The second part represents the core of the argumentation and it is constituted by Chapters 3 and 4, respectively Methodology and Results. Taking into account the goals of the research activity, the analyzed case is firstly exposed, emphasizing the main figures of merit, algorithms and operation of developed codes; then the obtained results are presented and analyzed with particular regard for gain profile characteristics.
The last part is related to Chapter 5 - Conclusions - where purposes are compared to the obtained results, commenting on their meaning and evaluating the progress with respect to the previous ones. Further possible prosecutions of the research are proposed, even in prospective of field experimentation.

Chapter 2

Introduction on Optical Communication Systems

The aim of the following section is to introduce the reader to the world of optical communications, explaining the fundamental elements that compose an optical communication system and mentioning the overall operation.
Going into details, the discussion prosecutes with the description of Raman effect and its applications in optical amplifiers, showing the principal types and putting in evidence characteristics and their respective advantages.

2.1 Preliminary concepts

In the Internet age, the current society results to be more and more connected thanks to the use of objects and applications that allow to execute each kind of task exploiting the communication and exchange of data through the network.

Figure 2.1: Overview of optical fiber links under the sea.

Internet is the combination of two types of networks. The first ones are back bones networks which are used to transfer information for long paths around the globe

and they are constituted by high-capacity optical links. The second ones are access networks which represent the last step of the communication chain toward the user and they can be implemented through wireless or wired systems.

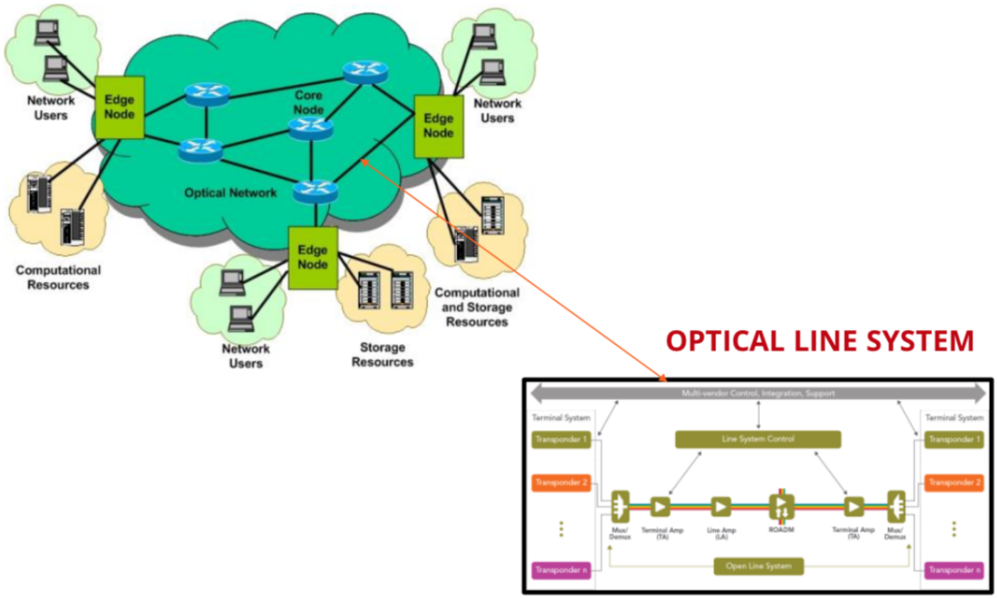

Figure 2.2: Scheme of an optical network.

Every year, the number of internet users increases sharply, arriving to more than 4 billion people in January 2019 [12], and concurrently also the global IP traffic increases [5].
In this prospective, the further challenge is to improve the existing network trying to maximize performance and exploiting the maximum capacity that optical line systems can provide.

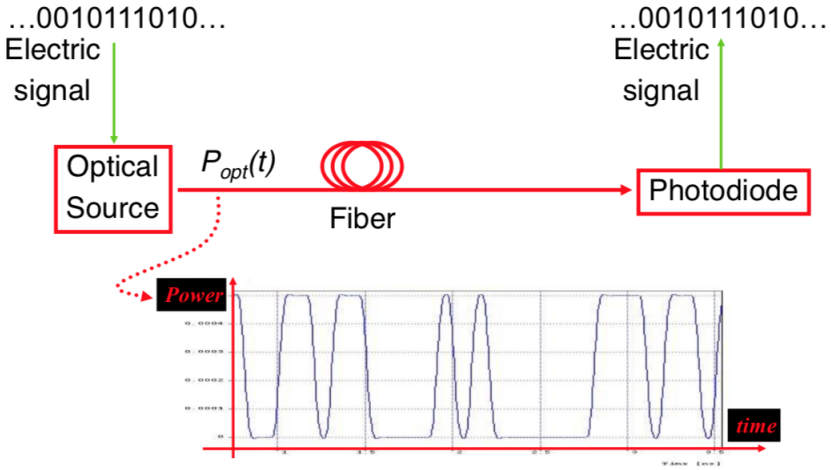

Figure 2.3: Basic operation of an optical communication system.

In figure 2.3, the basic operation of an optical communication system throughout the use of the fundamental components is represented.
Generally, a coherent optical source as a LASER beam is modulated varying the power intensity between the ON and OFF states, which can be encoded through the

use of binary values '0' and '1'. This technique is called on-off key modulation and it is first and the simplest optical communication strategy adopted. The current modulation formats used in state of art systems are based on coherent modulation [13].
The electromagnetic field is then propagated through the optical link and arrives to the receiver side which provides for sensing and sampling the photonic beam in order to extract information.

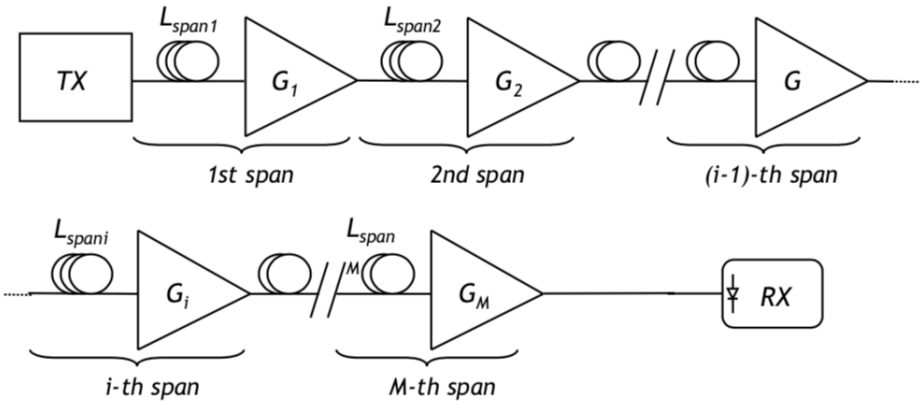

$$L = \sum_{i=1}^{M} L_{span,i}$$

Figure 2.4: Block scheme of optical line system.

Focusing on the optical link, it is generally a cascade of building blocks, each one constituted by a couple fiber-amplifier. So, the overall length of the optical link is the sum of the lengths of each span, as represented in figure 2.4.

Optical fiber and amplifier characteristics will be described more in details in the following subsections. Now, the basic physical principles which allow transmission along an optical fiber are mentioned.

When an electromagnetic field interacts with a dielectric material, it undergoes three main effects:

- Attenuation along the dielectric medium;
- Refraction and reflection due to presence of the interface between two dielectric materials;
- Material dispersion.

When an electromagnetic field propagates along a dielectric material, it attenuates according to an exponential law with respect to the distance (fig. 2.5):

$$P(z) = P(0)e^{-2\alpha z}$$

where $P(0)$ is the input power of the electromagnetic field and α is the loss coefficient expressed in linear units [km^{-1}].

Having fixed the distance at 1 km, the loss coefficient can be expressed also in $[\frac{dB}{km}]$:

$$\alpha|_{dB/km} = 10 \log_{10}(\frac{P_{in}}{P_{out}})|_{1\,km}$$

and from it:

$$P(z)|_{dBm} = P(0)|_{dBm} - \alpha|_{dB/km} \cdot z$$

Currently, optical fiber manufacture is able to produce models which have loss coefficients below 0.2 dB/km at 1550 nm.

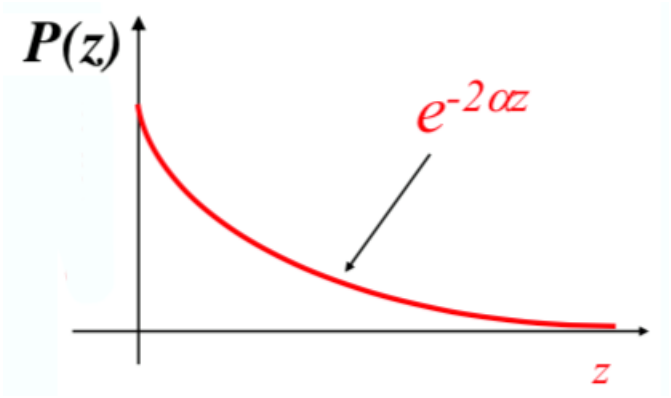

Figure 2.5: Electromagnetic power propagation along a dielectric material.

The refractive index n of the dielectric material affects the speed of the electromagnetic field ν:

$$\nu = \frac{c}{n}$$

where c is the light speed in the vacuum. In the glass, the electromagnetic field speed is about two third of that in the vacuum.
Considering the interface between two dielectric materials with different refractive indices n_1 and n_2, when an electromagnetic field impacts on it, transmitted and reflected electromagnetic fields that derive from the interaction answer to the following laws (fig. 2.6):

- Reflection law:

$$\theta_i = \theta_r$$

- Snell's law:

$$n_1 \, sin\, \theta_i = n_2 \, sin\, \theta_t$$

where the reflection angle θ_r is the one between the black dashed line orthogonal to the interface and the red dashed reflected ray.
Light propagation inside on optical fiber is possible thanks to the phenomenon of the total internal reflection.
Assuming that $n_1 > n_2$, the critical angle for which there is only the reflected ray and no transmitted ray can be computed through the Snell's law:

$$\theta_c = arcsin(\frac{n_2}{n_1})$$

The refractive index n is a parameter that varies according to other properties of the electromagnetic field. In particular, it depends on the wavelength or the frequency

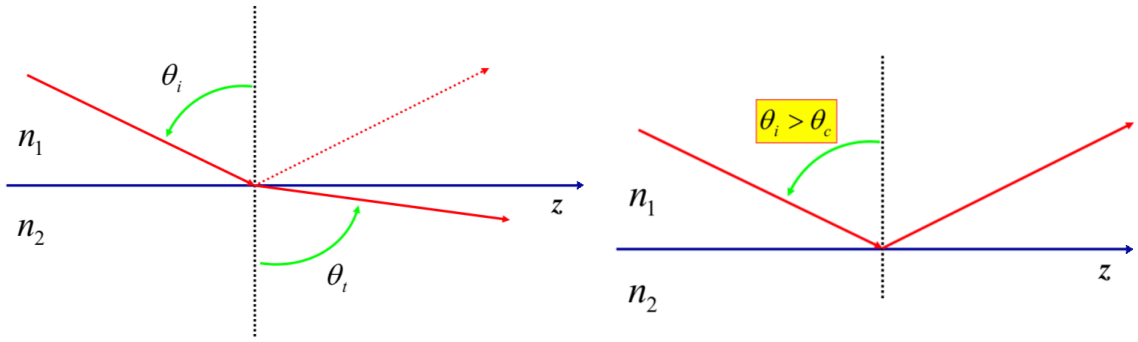

Figure 2.6: Snell's law and total internal reflection graphic representation.

of the electromagnetic field that propagates inside the dielectric material. In fact, the speed of the light beam changes according to its wavelength. For this reason, the phenomenon takes the name of *material dispersion*.

2.2 Optical fiber

What allowed the real revolution in telecommunications through the use of glass optical fibers in wired communication systems was an intuition of Prof. K. C. Kao [11]. In 1966, he published his demonstration of the fact that glass could be made pure and transparent enough to decrease fiber losses and to exploit it as waveguide material. Shortly thereafter, optical fiber did not find other competitors in terms of performances and they determined the development of the scientific progress in optical communication field, also thanks to the invention of LASER [9], [1].

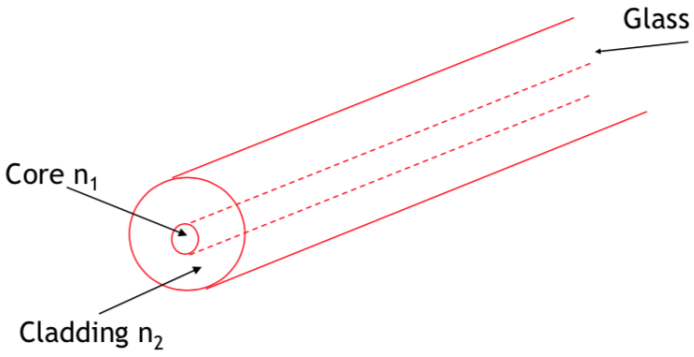

Figure 2.7: Basic representation of an optical fiber.

Generally, an optical fiber is an extremely thin wire with circular section commonly made in glass (fig. 2.7). It is composed by two parts, the core, which is the internal cylinder with an higher refractive index, and the cladding which is the external cover.
The choice of glass as optical fibers material is due to the fact that at optical frequencies it maintains a reasonably low attenuation. Typically, the core refractive index is made higher thanks to a doping process [15].

In figure 2.8, the attenuation of a typical optical fiber with respect to frequency is reported.

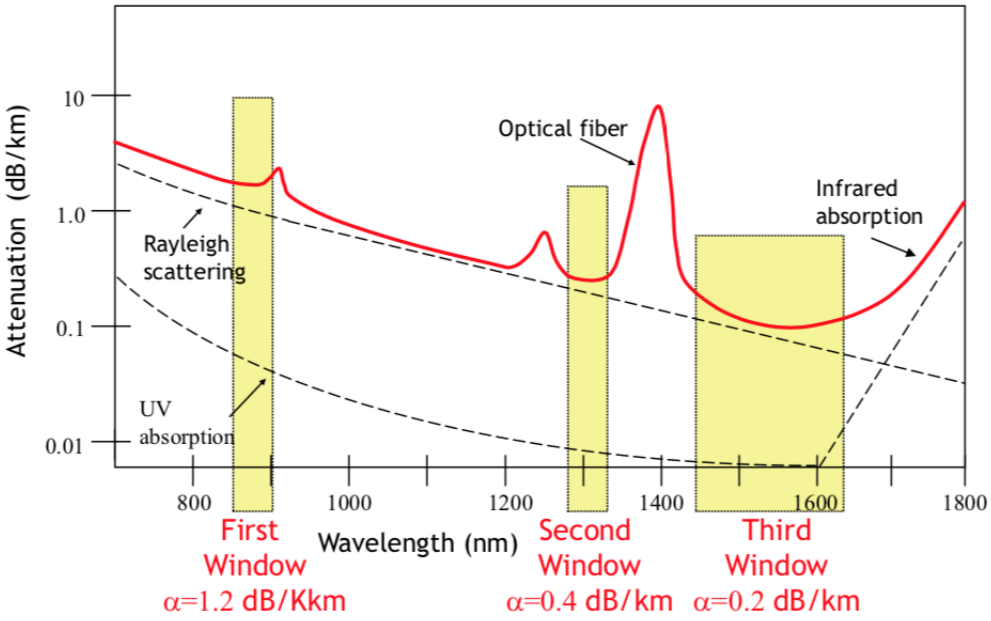

Figure 2.8: Attenuation of the fiber with respect to frequency.

Frequency ranges that present almost constant values of attenuation are called windows. Traditionally, they were object of progressive investigations in the last 50 years according to the technology and the instrumentation available.
In state-of-the-art optical fiber technology, attenuation at 850 nm reaches entities of the order of about 2 dB/km. At the second window (1300 nm) typical attenuation is of the order of 0.5 dB/km. The third window corresponds to the union of S band, C band and L band (from 1460 nm to 1625 nm) and in this frequency range there is the global minimum of the attenuation curve. In particular, recent studies have brought the minimum attenuation of the fiber to extremely low values below 0.16 dB/km [19]. Generally, a commercial optical fiber has attenuation values around 0.2 dB/km at 1550 nm.

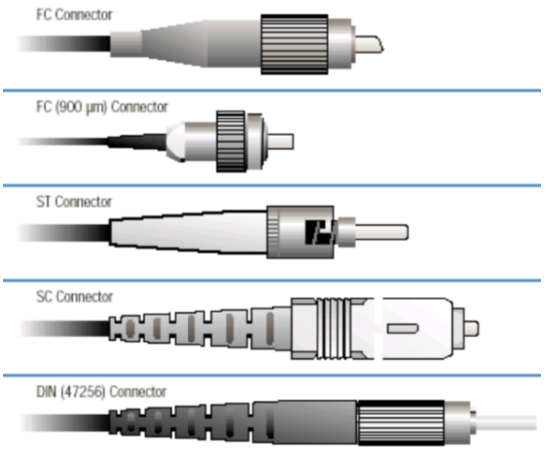

Figure 2.9: Typologies of fiber connectors.

Furthermore, fiber attenuation is not the unique factor that contributes to lower the electromagnetic field power. Connectors are frequently used in order to join consecutive fiber spans (fig. 2.9), introducing insertion losses which can arrive until 0.5 dB.

In order to reduce this lumped attenuation, fusion slice techniques are used in order to perform fiber-to-fiber coupling, achieving insertion losses even lower than 0.1 dB.

For high-performance optical communication purposes, generally single-mode step-index fibers are adopted (fig. 2.10).

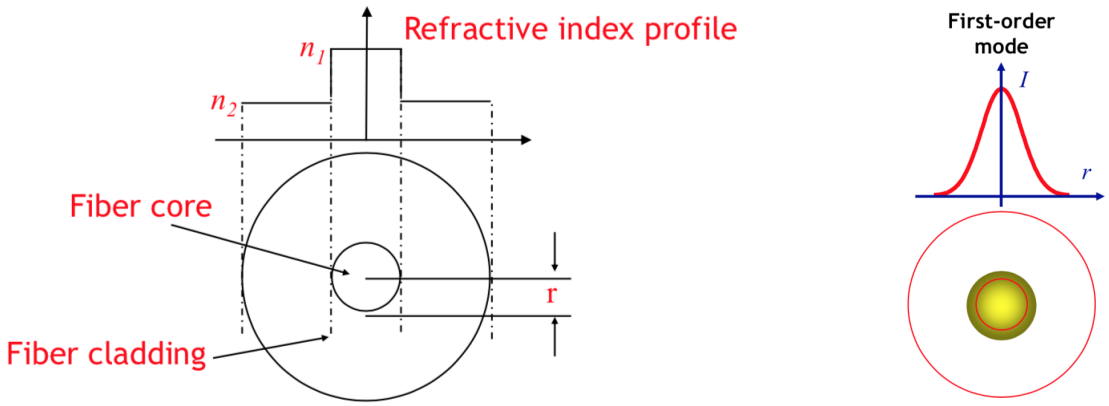

Figure 2.10: Step-index single-mode optical fiber.

This kind of fibers present a constant piece-wise refractive index profile passing from the cladding to the core with a significant and sharp variation. It is possible to define an important parameter for step-index fibers called relative refractive index or contrast, defined as follows:

$$\Delta = \frac{n_1 - n_2}{n_1}$$

It is extremely important for the confinement of the electromagnetic field inside the optical fiber.
In general, total internal reflection phenomenon inside the optical fiber is related to the entity of the relative refractive index Δ and the incidence angle θ_i.
Single-mode fibers are used in order to avoid intermodal dispersion [4], maintaining high performance in terms of switching electromagnetic pulses velocity. The name of this type of fibers is usually abbreviated with the acronym SMF and the typical dimensions of the core and the cladding are respectively of about 10 μm and 125 μm. The whole structure of the optical fiber is then composed by a sequence of further layers in order to prevent mechanical stresses which can occur during the placement and the operation of the component (2.11).

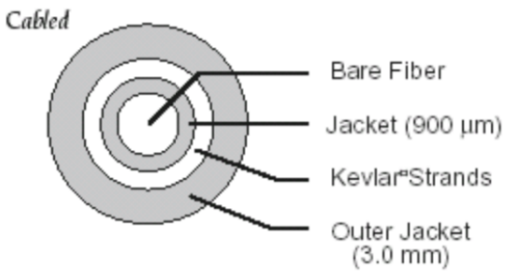

Figure 2.11: Structure of an optical fiber.

Usually, multiplexing techniques are implemented in order to send concurrent multiple data on the same link in optical transmission systems. The two techniques that are effectively used for applications are:

- Time Division Multiplexing (**TDM**);
- Wavelength Division Multiplexing (**WDM**).

The first kind of multiplexing method is the same used to transmit data streams coming from different channels on a single bus. In each time slot, a portion of every channel data is present.

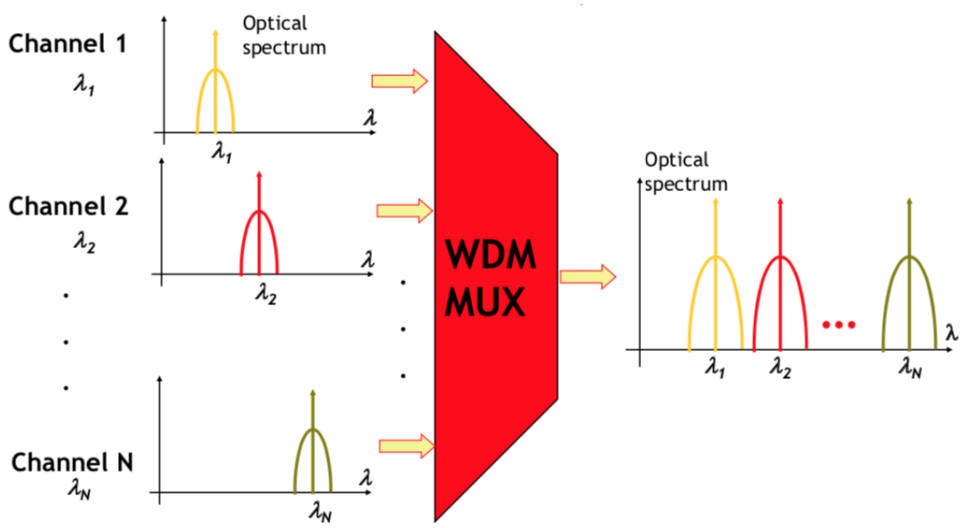

Figure 2.12: Wavelength Division Multiplexing technique.

On the other hand, the WDM technique combines on the same physical link channels which have different central wavelengths or frequencies. In general, this device is realized with a passive device such as an optical filter or coupler (fig. 2.12). It is very suitable for optical fiber which is an high-capacity medium with respect to frequency.
There are two different approaches for WDM according to applications and requests:

- Coarse WDM (CWDM);
- Dense WDM (DWDM).

The first one exploits a limited number of channels, usually a few tenths, with a large spacing in frequency. The second one, instead, adopts many channels with a narrow frequency spacing, getting to use even hundreds of channels [7].

At the receiver side, WDM channels are separated in order to derive information from each one of them adopting a multi-port filter.

2.3 Raman amplifiers

The Raman effect takes the name from its discoverer Prof. C. V. Raman for which he won the Nobel prize in 1930 [17].

The physical mechanism is related to the interaction between a photonic beam and the molecules of the material in which it is propagating. When a photon collides with a molecule, this one acquires energy and can reach a higher energy level. After the energetic adjustment, the interaction has as products a scattered photon at lower frequency which depends on the medium and a phonon with characteristics related to the difference in frequency among the incident photon and the scattered one. These optical components shifted at lower frequency with respect to the initial photon frequency are called Stokes waves [2].

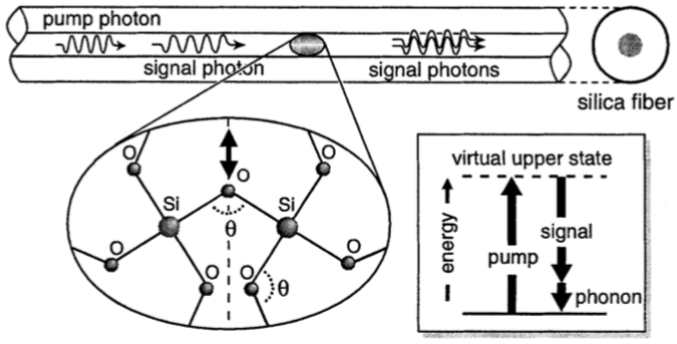

Figure 2.13: Representation of optical amplification due to stimulated Raman scattering along a silica fiber [2].

A particular kind of Raman scattering takes place when the frequency difference of two photon beams is within a certain range: Stimulated Raman Scattering (SRS). In this case, it is possible to notice a coherent optical amplification effect through a power transfer from signals at higher frequencies to signals at lower frequency and additional vibrational energy related to release of phonons.
This phenomenon is present in every material; in particular, in silica it mostly depends on the Si-O-Si bounds (fig. 2.13).

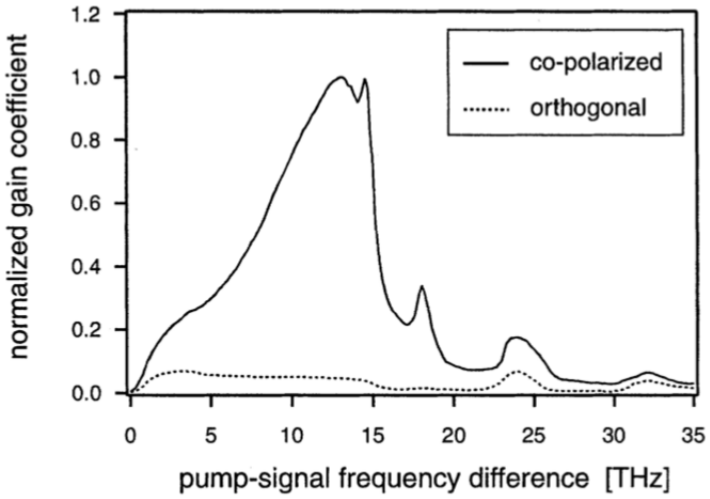

Figure 2.14: Raman efficiency curves calculated in base on different pump and signal polarization [2].

The entity of the Stimulated Raman Scattering is described by the Raman efficiency curve of the medium, highlighting the strength of the interaction according to the frequency separation among photon beams. It is a polarization dependent process (fig. 2.14). Generally, the discrepancy among co-polarized and orthogonal photon beams is about an order of magnitude.
Moreover, Stimulated Raman Scattering does not depend on the propagation direction of the two interacting optical signals. So, power transfer occurs always either for co-propagating signals or for counter-propagating signals.

For the purpose of this work, the interest is focused on two main consequences of the Raman effect in optical communication applications:

- Raman cross-talk;
- Raman amplification.

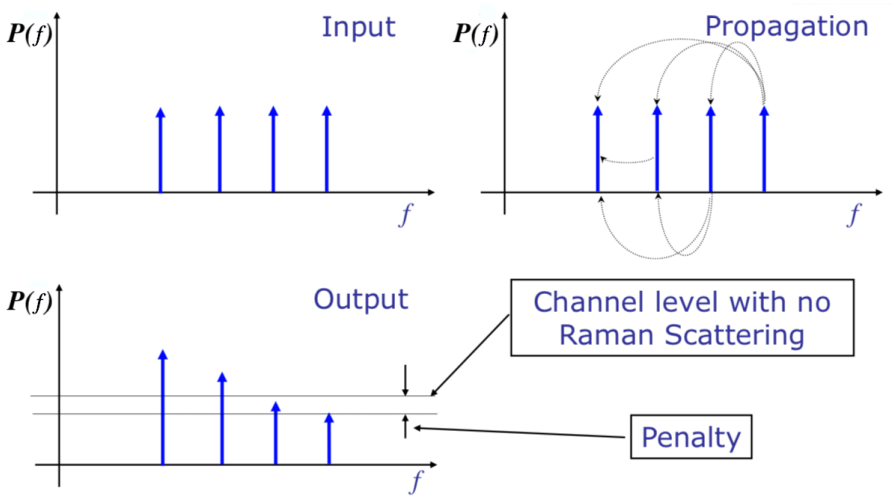

Figure 2.15: Mechanism of Raman cross-talk.

The first one is a drawback found in WDM systems, due to the fact that the input spectrum that is loaded on the optical fiber has signals at different frequencies. During the propagation, signals at higher frequencies have a pumping effect on those at lower frequencies, having as final result a tilting effect (fig. 2.15).

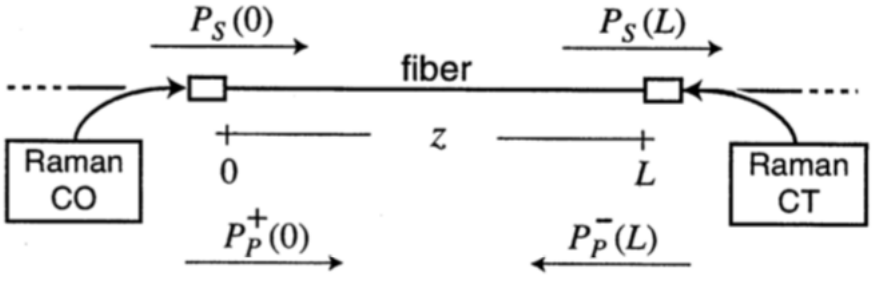

Figure 2.16: General scheme of a Raman amplifier [2].

On the contrary, Raman amplification is the exploited in order to obtain a distributed amplification along the optical fiber.

In figure 2.16 the representation of a general Raman amplifier is reported.
A certain number of high-power signals at higher frequency with respect to the WDM ones are introduced inside the optical fiber. Those are called pumps and they are used to transfer power to the modulated signals and to obtain the wanted amplification (fig. 2.17).

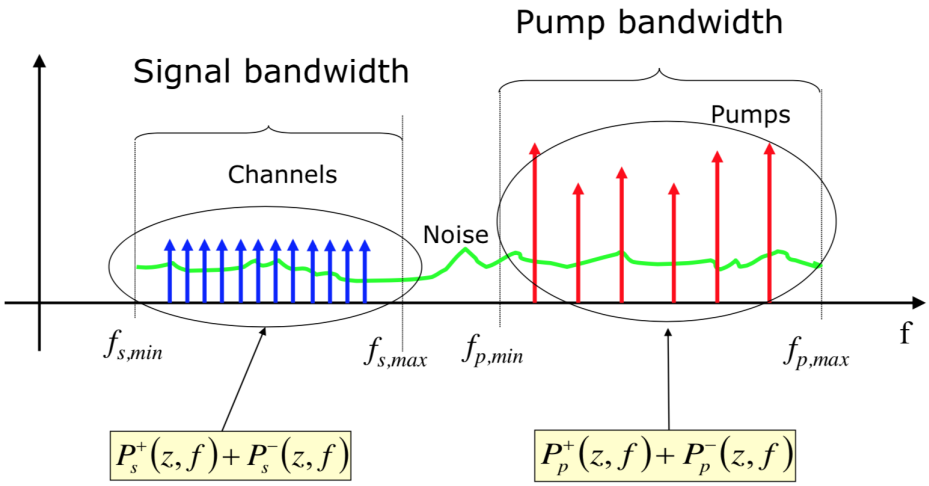

Figure 2.17: Spectrum with WDM signals and Raman pumps.

Raman amplification determines also the production of noise. In this case, amplified spontaneous emissions (ASE) is the dominant contribution of noise and it is a natural consequence of the amplification.

Thanks to figure 2.18, it is possible to understand the contributions given to signals by each set of co-propagating and counter-propagating Raman pumps. In particular, Raman interaction occurs when the entities of Raman pumps powers are significantly large. In this way, co-propagating pumps enhance signals power at the beginning of the fiber, while counter-propagating pumps have the same behaviour at the end of the fiber.

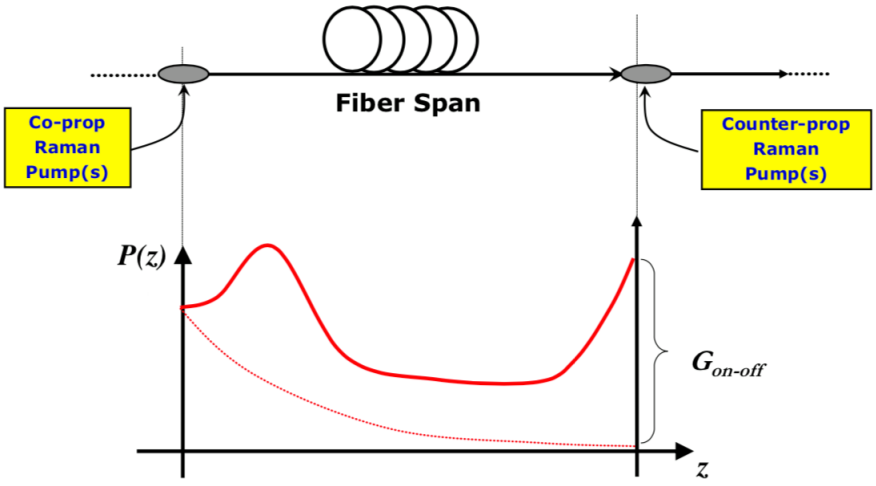

Figure 2.18: General operation of a Raman amplifier.

In general, Raman amplifiers are adopted in optical communication systems because it is a phenomenon that occurs in every kind of optical fiber. It is also a wide-band amplification, so it is extremely useful in scenarios where multi-band transmission is needed. Moreover, the noise accumulation along fiber spans is lower than systems which adopt only EDFAs and this allows to propagate information along longer spans. [2], [8], [14].

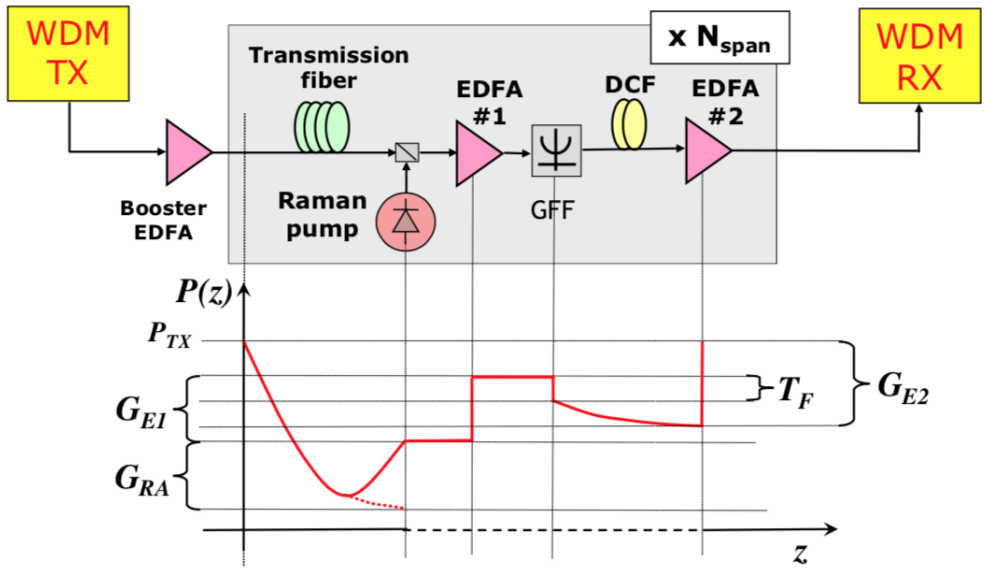

Figure 2.19: Scheme and operation of hybrid Raman/Erbium-Doped Fiber amplifiers [3].

In conclusion, recently, complex designs of hybrid amplifiers have been done in order to optimize gain performances, to keep noise accumulation controlled, to mitigate fiber nonlinearities [3].
Starting from these premises, the main purposes are to extend the transmission band, moving to Dense Wavelength Division Multiplexing systems, and to maximize single span length of the whole optical link path.

Chapter 3

Methodology

The following chapter presents the fundamental algorithms that constitute the basics of the whole framework. Generally, two kind of algorithms were implemented:

- Algorithms for optimization;
- Algorithms for the analysis of the optimum solution.

Given a certain preliminary physical description of the scenario under analysis, all developed codes and functions have as primary engine an emulator that allows to evaluate the consequences of Raman effect: the Raman Solver.
This examination brings to clarify the structure of the work so that every result that will be seen afterwards could be easily analyzed and evaluated knowing the methodology behind its derivation.

The entire framework is developed in Python 3.7, having as starting point other codes that will be presented below. The choice of this programming language is due to many factors. In addition to the many advantages and the credit that it had obtained in recent times, Python is an open-source language, which has benefits from the community and from the possibility of sharing pieces of codes and knowledge among users. This characteristic has been fundamental for developing the present work, but it also helps the prosecution of the research for improving what was done and for trying to investigate new cases of interest.

3.1 Scenario under analysis

As first step, the scenario under analysis is described, presenting the physical and structural composition of the equipment and proposing an equivalent systemic representation.
A general scheme of the emulated scenario is reported in fig. 3.1. The equipment is constituted by three main elements:

- The input WDM power spectrum;
- The fiber link span;
- The Raman pumps.

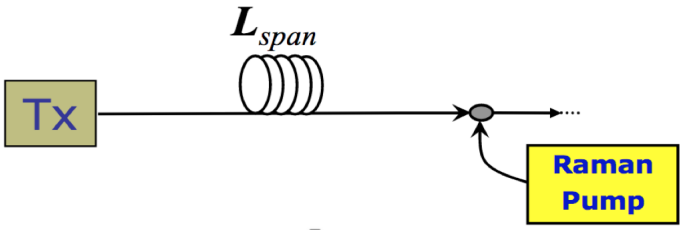

Figure 3.1: General block scheme of the emulated equipment.

The equivalent block scheme is reported in fig. 3.2.
Given a certain input power spectral density $S_{in}(f)$ at the begin of the fiber span, it is possible to derive the relative output power spectral density $S_{out}(f)$ at the terminal considering the linear combination of the contribution related to the fiber attenuation and Raman amplification $\rho(f, z)$ and the noise introduced by Raman pumps $S_{ASE}(f)$.

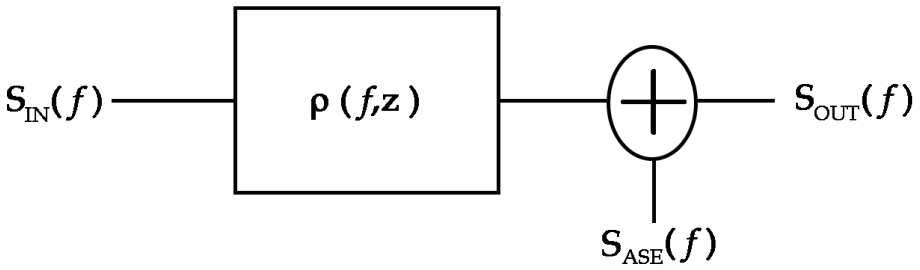

Figure 3.2: Equivalent block scheme.

In the analysis carried out, the scenario maintains the following characteristics:

- The input spectrum is selected choosing between two different patterns:
  - **C band**: it is composed by 96 channels in the range $[191, 196]$ THz;
  - **C+L band**: it is composed by 192 channels in the range $[186, 196]$ THz, with a frequency distance between L and C band of about 200 GHz.

  Each channel is spaced of 50 GHz with respect to its own central frequency from the adjacent ones and is assumed to be modulated with a 32 GBaud PM-16QAM signal with a 10% roll-off root raised cosine spectrum. The whole spectrum is always full loaded with a certain input power per channel.

- The link is a single-mode-fiber span of fixed length of about 120 km and the attenuation is modelled as a piece-wise function:
  - **Spectrum loss coefficient** (in the range [186, 197] THz): $\alpha_s = 0.21$ dB/km;
  - **Raman pumps loss coefficient** (in the range [197, 207] THz): $\alpha_p = 0.25$ dB/km.

- Raman amplification is made using two different sets counter-propagating Raman pumps placed at the end of the line that, according to the case, can be constituted by 4 or 5 pumps.

3.1.1 Figures of merit

From a mathematical point of view, having fixed the length of the fiber span, some reasonable parameters are pointed out from the system transfer function (fig. 3.3):

- The total attenuation of the fiber $A(f)$;
- The Raman pumps equivalent gain $G_{eq}(f)$;
- The Raman pumps equivalent noise figure $NF_{eq}(f)$.

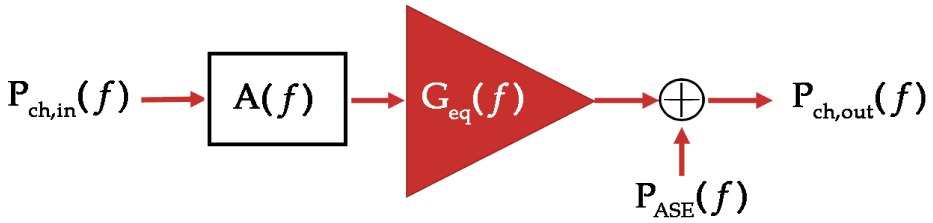

Figure 3.3: Equivalent block scheme having the fiber span length fixed.

The total attenuation $A(f)$ is a fundamental parameter to understand how much the amplifier has to recover in terms of signal power to propagate correctly the information. It is computed in linear units by the formula

$$A(f) = 10^{-[\frac{\alpha_s(f)}{10}]L_{span}}$$

where α_s is the loss coefficient of the signal measured in dB/km and L_{span} is the length of the fiber link in km.

Because the system does not present EDFAs, under this condition Raman pumps equivalent gain $G_{eq}(f)$ coincides with the on-off gain and it can be defined in linear units as:

$$G_{eq}(f) = G_{OO}(f) = \frac{P_{OUT,pumpsON}(f)}{P_{OUT,pumpsOFF}(f)}$$

where $P_{OUT,pumpsON}$ is the power per channel at the end of the line when Raman pumps are active, and $P_{OUT,pumpsOFF}$ is the power per channel at the end of the line when the Raman pumps are turned off.
As a consequence, the on-off gain represents the scale factor that allows to reach the required signal power level, given a certain set of Raman pumps.

On the other hand, the equivalent noise figure $NF_{eq}(f)$ is evaluated exploiting the definition of ASE power:

$$P_{ASE}(f) = NF_{eq}(f) \cdot h \cdot f \cdot G_{OO}(f) \cdot B_r$$

and inverting the formula as follows:

$$NF_{eq}(f) = \frac{P_{ASE}(f)}{h \cdot f \cdot G_{OO}(f) \cdot B_r} \tag{3.1}$$

where h is the Planck's constant, f is the considered frequency, $G_{OO}(f)$ is the on-off gain and B_r is the reference bandwidth.
The equivalent noise figure $NF_{eq}(f)$ is an estimation of the contribution of the noise on a certain channel due to the specific Raman amplifier.

3.2 Raman solver

The starting point of the thesis activity and also the core of each code that has been developed is the Raman solver.
It is an open source framework and it is present in the GitHub repository of the Telecom Infra Project [16] (TIP).

Given a certain scenario, the Raman solver is a tool that allows to emulate the behaviour of the Raman effect according to the ordinary differential equations that describe the amplification [2]:

$$\begin{aligned} \frac{dP_s}{dz} &= -\alpha_s P_s + C_R(\lambda_s, \lambda_p)[P_p^+ + P_p^-] \\ \pm\frac{dP_p^\pm}{dz} &= -\alpha_p P_p^\pm - (\frac{\lambda_s}{\lambda_p})C_R(\lambda_s, \lambda_p)P_s P_p^\pm \end{aligned} \tag{3.2}$$

where α_s and α_p are the loss coefficients, C_R is the Raman gain efficiency of the fiber (fig. 3.4), that quantifies the strength of the coupling among pumps and signal, and $\pm$ shows if the Raman pump is co-propagating (+) or counter-propagating (-).

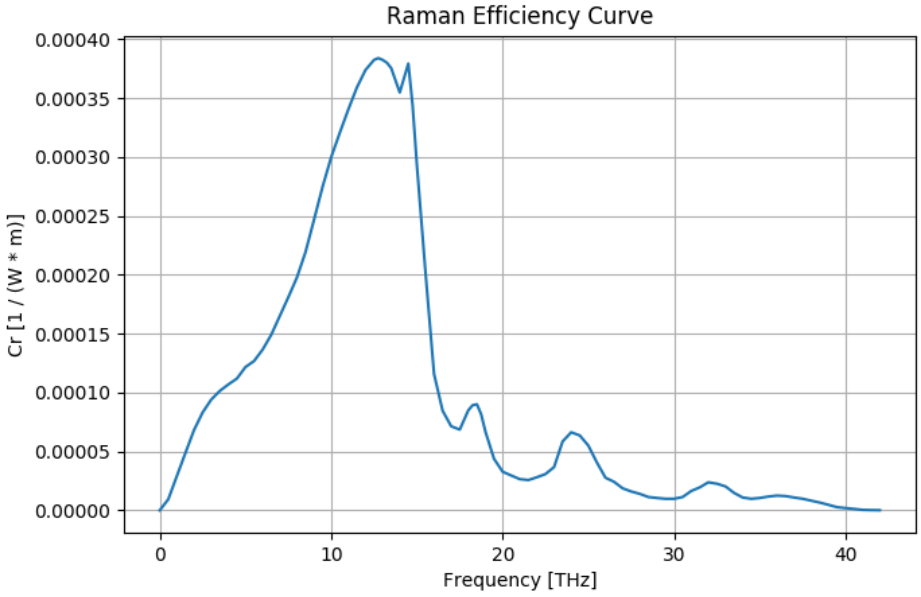

Figure 3.4: Raman efficiency curve adopted.

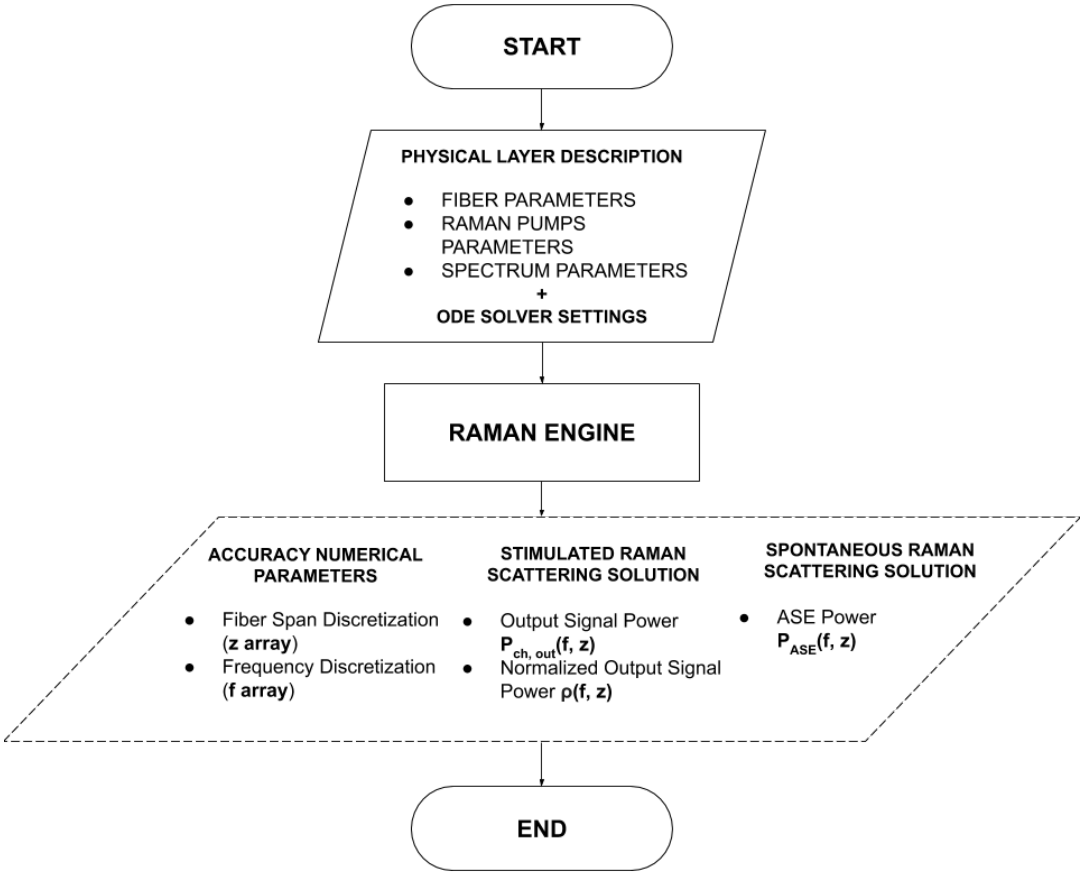

Figure 3.5: Raman solver flow diagram.

The contribution of the noise related to the ASE power is computed according to the formula:

$$\pm\frac{dP^{\pm}_{ASE}}{dz} = -\alpha_{ASE}P^{\pm}_{ASE} + C_R(\lambda_{ASE},\lambda_p)P_pP^{\pm}_{ASE} + C_R(\lambda_{ASE},\lambda_p)[1+\eta(T)]hf_{ASE}B_rP_p$$

where $P^{\pm}_{ASE}$ is the single polarization ASE power and $\eta(T)$ is the phonon occupancy, that depends on temperature T and also on the frequency separation between signal and pumps.

The Raman solver does not take into account NLI generation. Even if this phenomenon is an intrinsic effect of the fiber produced by the interaction between the electromagnetic field and the medium, in moderate pumping regime, it is possible to separate NLI and Raman contributions. Assuming that the Raman amplification does not recover the total attenuation of the fiber $A(f)$ (below transparency) condition, NLI is generated at the beginning of the fiber, where the spectrum power is much larger than Raman pumps power, and Raman ASE power is generated at the end of the fiber, where Raman pumps power is dominant with respect to signal power.

The flow-diagram reported in fig. 3.5 illustrates the procedure that brings to the correct evaluation of the Raman effect.

The Raman engine is the main program that executes the emulation. The user has to insert as input parameters the following information:

- **Fiber parameters**:
  - Loss coefficient function α;
  - Raman efficiency curve C_R;
  - Temperature T.
- **Spectrum parameters**:
  Channels which compose the input spectrum, described through:
  - Central frequency of each channel f_s;
  - Symbol rate;
  - Roll-off;
  - Input power per channel P_s.
- **Raman pumps parameters**:
  Set of Raman pumps, described through:
  - List of Raman pumps input powers P_p;
  - List of Raman pumps wavelengths λ_s;
  - List of Raman pumps propagation direction (co-propagating or counter-propagating);
- **ODE solver settings**:
  - Resolution along z axis;
  - Convergence tolerance;
  - Verbose.

Provided the previous input parameters, the Raman engine gives as outputs:

- **Accuracy numerical parameters**: arrays that contain the discretization of the solution in frequency and along the fiber link (z axis);
- **Stimulated Raman Scattering solution**: matrix of values containing the evolution of the power per each channel along the z axis;
- **Spontaneous Raman Scattering solution**: matrix of values containing the evolution of the ASE power per each channel along the z axis;

In the next analysis, the Raman solver will be fed with different data according to the kind of research to operate, maintaining unchanged the data set.

3.3 Examples of emulation

The Raman solver can be used to study a wide range of cases. So, it is fundamental the comprehension of the potentialities of this tool trying some examples of emulation, in order to observe typical types of graphs that will be useful for the presentation of results related to the research activity.

In this section, the attention is focused on the observation and the meaning of the solution come out from the Raman solver, without the necessity to have an exhaustive description of the case.

3.3.1 Propagation along the fiber

Given a fiber span of 100 km and an input spectrum loaded with 91 channels in C band, the effect of a single counter-propagating pump with 0.5 W of input power at 207 THz is emulated.
In fig. 3.6, the propagation of channels power and and pump power along the fiber link is graphically reported. In this case, the normalized power $\rho(f, z)$ has been taken into account.
The fiber transfer function including attenuation and stimulated Raman scattering (bunch of multicolored lines) is defined as:

$$\rho(f, z)_s = \sqrt{\frac{P_s(f, z)}{P_s(f, 0)}}$$

where $P_s(f, 0)$ is the input power of spectrum. Similarly, the same feature is defined for Raman pump power (single orange line) as:

$$\rho(f, z)_p = \sqrt{\frac{P_p(f, z)}{P_p(f, L_{span})}}$$

where $P_p(f, L_{span})$ is the input counter-propagating Raman pump power.

At first glance, it is possible to notice the effect of distributed amplification that the Raman pump has on the signal spectrum. Since the emulation is carried out for two different values of input power per channel, -3 dBm and 3 dBm, in the second case the trend of the pump power is not decreasing exponential (decreasing linear in logarithmic scale) as the first one. This effect is the called pump depletion and it is described in equation 3.2 through the second term of the expression, in which the product between pump power and signal power is contained. For high levels of signal power, the power transfer from pumps to spectrum is enhanced and the decay of the pumps power trend is sharped for this reason. In some cases, as the first one, pump depletion can be negligible (undepleted pump assumption) due to the low entity of the signal power, having a behaviour along z axis of the pump power that is linear adopting the semi-logarithmic scale.

Spectrum profiles at the end of the line ($z = L_{span}$) of the same scenario are reported in fig. 3.7. Thanks to this graph, it is possible to appreciate some fundamental properties of the Raman effect.

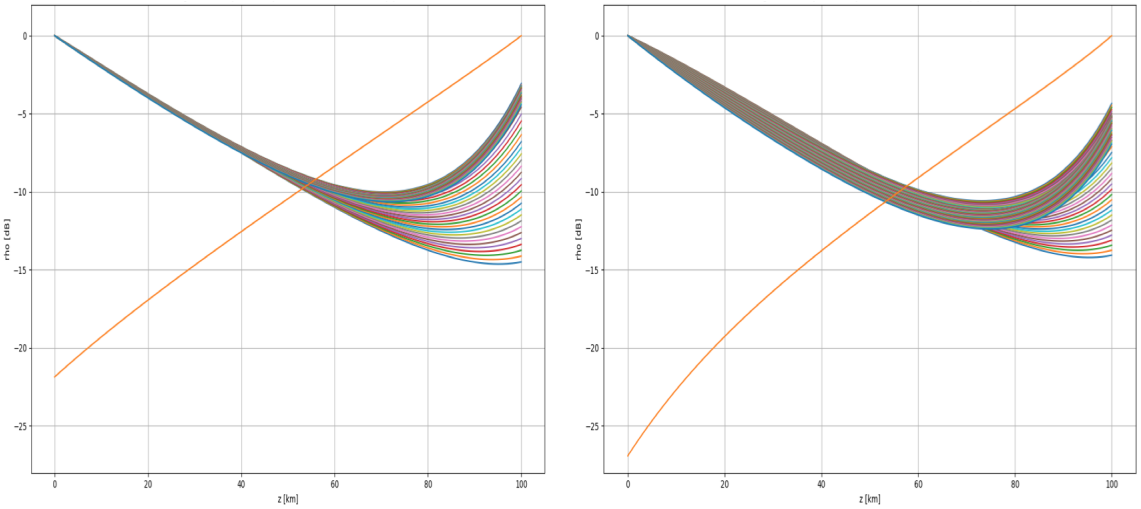

Figure 3.6: Propagation along z of pump power and input signal pattern (-3 dBm and 3 dBm).

The impact of Raman efficiency curve (fig. 3.4) is clear when Raman pump is active (blue lines), observing the presence of the main two peaks.
In the scenario with turned-off pump, and so without Raman amplification, the flat spectrum profile is tilted and its slope depends on the amount of input power per channel (higher slope for higher power level). This phenomenon is called inter-channel Raman effect and it is a consequence of the presence of adjacent channel at different frequencies that exchange power transferring it from channels at higher frequencies to channels at lower frequencies. It is also called Raman cross-talk due to the fact that adjacent channels are not completely isolated, but they exchange a certain amount of energy.
Furthermore, the overlapping of the spectrum profiles with turned on and off pump at the end of the line suggests the definition of on-off gain, which is exactly the different between the two curves in logarithmic units.

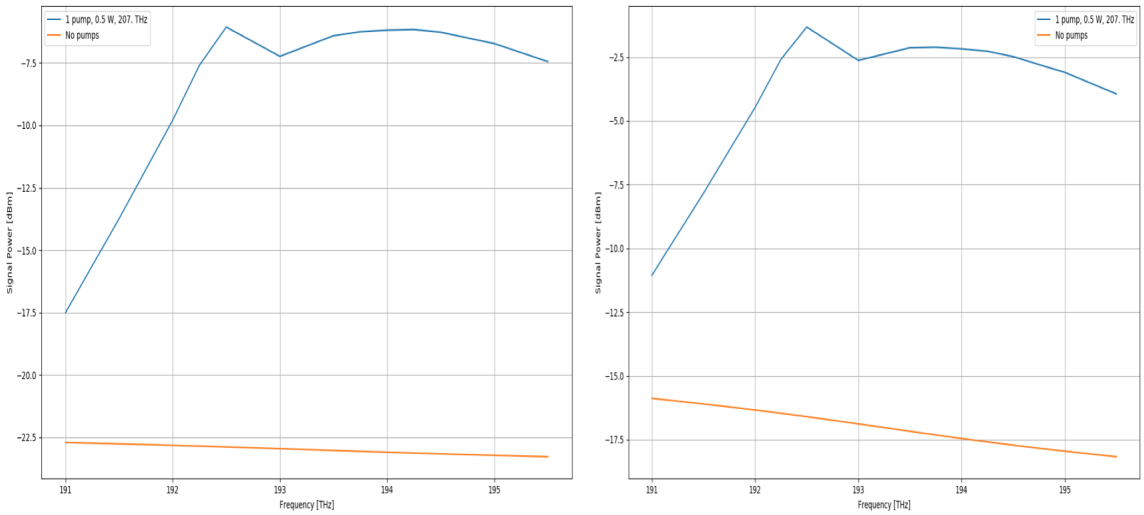

Figure 3.7: Power profile of the input signal pattern at the end of the fiber span (-3 dBm and 3 dBm).

Now, the pumps depletion is observed on a scenario with 4 Raman pumps changing the level of input power per channel. In figures 3.8, 3.9 and 3.10 power propagation along the fiber of the Raman pumps and the relative gradient evaluation are reported.
Thanks to the gradient evaluation via incremental ratio computation, it is quite straightforward how the depletion is more evident increasing the input power level per channel.
In the first case ($P_s(f) = -10$ dBm), at the end of the pumps power propagation (begin of the line for the input spectrum) all trends settle at the slope of the fiber loss coefficient for pumps $\alpha_p = 0.25\,dB/km$. Increasing the power spectrum level, the slope of the pumps powers increase as well and the pumps depletion becomes even more reasonable.
On the other hand, at the begin of the propagation of pumps powers (end of the line for the spectrum power), it is evident the pumping effect that pumps placed at higher frequencies have on pumps at lower frequencies. In fact, the power level of the pump at lower frequency (higher wavelength) becomes the most significant, receiving power from pumps at higher frequencies.

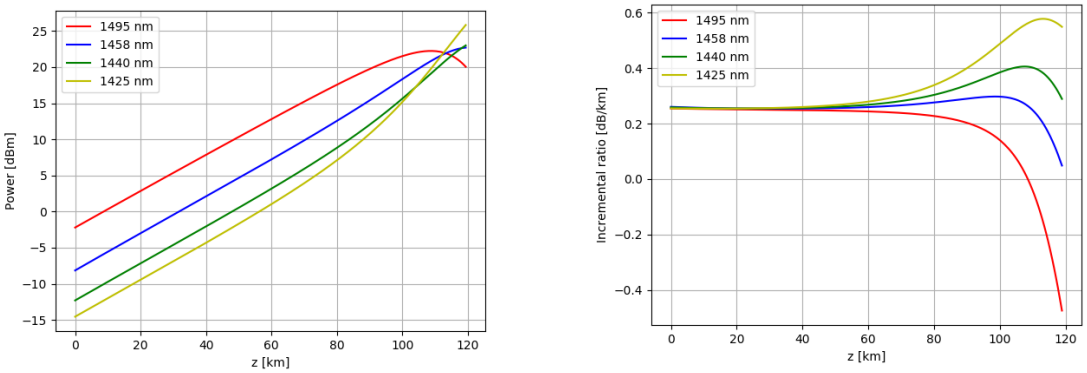

Figure 3.8: Propagation along z axis of pumps power and incremental ratio evaluation, -10 dBm of input power per channel (undepleted pump assumption).

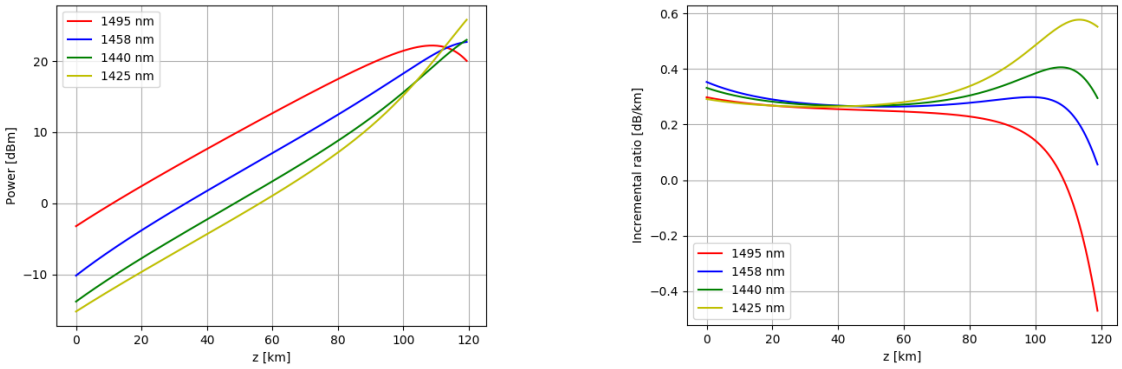

Figure 3.9: Propagation along z axis of pumps power and incremental ratio evaluation, 0 dBm of input power per channel.

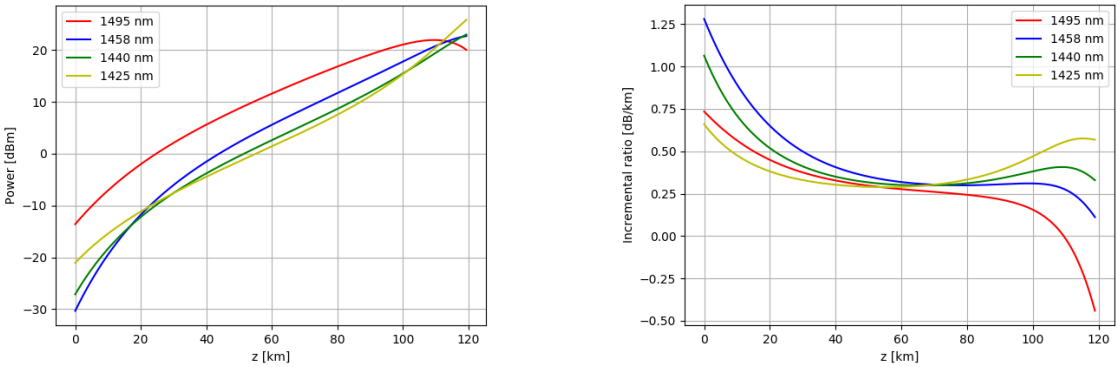

Figure 3.10: Propagation along z axis of pumps power and incremental ratio evaluation, 10 dBm of input power per channel.

3.3.2 On-off gain and noise figure

In this last example, the reliability of the Raman solver is tested, comparing its solution with emulation results coming from the analytic solution in undepleted pump assumption and another already tested solver written in C.

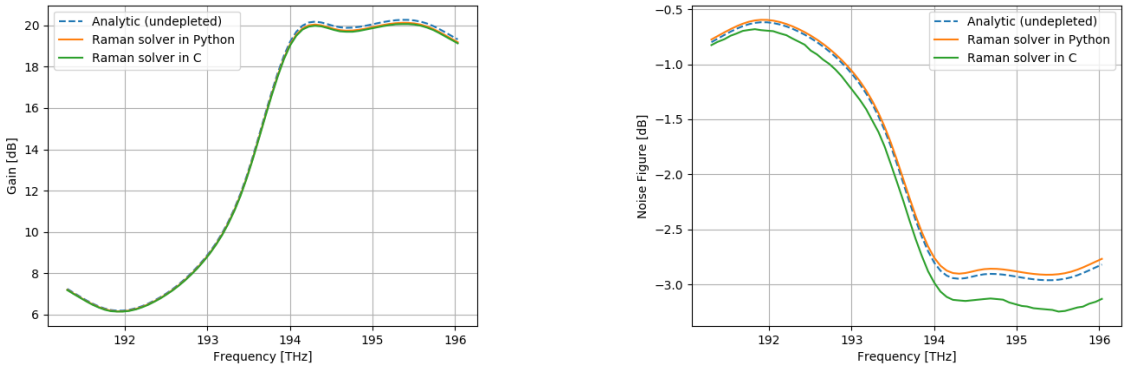

Figure 3.11: Gain and noise figure profile (-10 dBm, undepleted pump assumption).

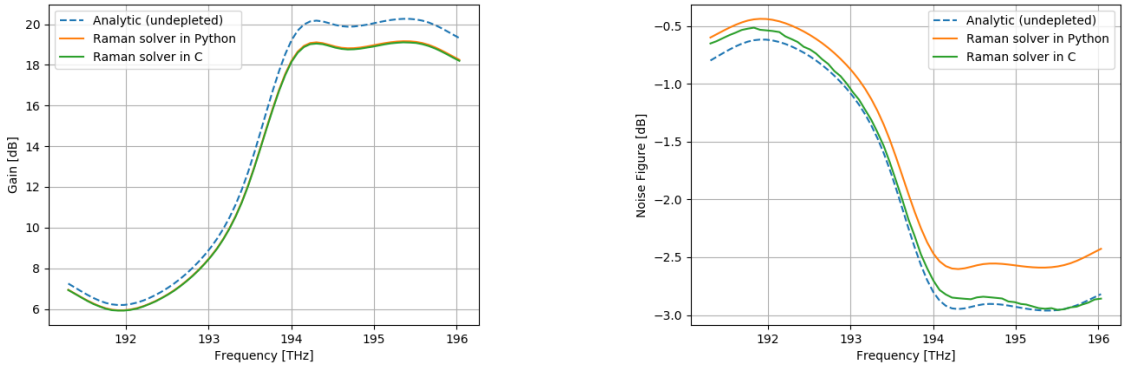

Figure 3.12: Gain and noise figure profile (0 dBm).

Considering the undepleted pump assumption, the analytical solution exploits the following formulas for the on-off gain:

$$G_{OO}(f) = exp\left\{C_R(f)P_{pump,IN}\frac{1-exp[-\alpha_p L_{span}]}{\alpha_p}\right\}$$

where α_p is loss coefficient for Raman pumps in Neper/km, and for the noise figure the formula is the same of 3.1 computing the ASE power as follows:

$$P_{ASE}(f) = B_r h f C_R(f) G_{OO}(f) e^{-\alpha_s L_{span}} \int_0^{L_{span}} P_p(\zeta) G_{RA}^{-1}(\zeta, f) d\zeta$$

where $G_{RA}(z, f)$ is the Raman gain evolution along the fiber span, defined as:

$$G_{RA}(z, f) = \frac{P_s(z, f)}{P_s(0, f)} = exp\left\{\int_0^z [C_R(f) P_p(\zeta) - \alpha_s(f)] d\zeta\right\}$$

Given a fiber span of 100 km, an input spectrum loaded with 64 channels in C band and a single counter-propagating pump with 0.55 W of input power at 1435 nm, on-off gain and noise figure profiles of the three emulators are overlapped in figures 3.11 and 3.12, considering two levels of spectrum input power, -10 dBm and 0 dBm.

Observing the on-off gain profile, all solutions practically coincides for -10 dBm of input signal power and this is correct because the case respects the undepleted pump assumption. Increasing the input signal power at 0 dBm, solutions of the two emulators vary in the same way with respect to the analytical one due to the fact that pumps depletion is not taken into account.
Then, considering the noise figure profiles, the same behaviour of the on-off gain is observed; the only difference is related to an apparent offset between the two emulators' solutions that is in any case less than 0.3 dB.
Being developed for other purposes, the solver written in C presents a slightly different solution in terms of numerical results with respect to the Python solver. It is probably related to the implementation of the software, tolerance settings and resolution.

With this last example of emulation, the reliability of the Raman Solver has been demonstrated. It is able to follow with an high level of accuracy the analytical solution in undepleted pump condition and to emulate the inter-channel Raman effect and the depletion of Raman pumps. Furthermore, an overview of the possible kind of results has been completed, making simpler the reading and the comprehension of the results in chapter 4.

3.4 Brute force strategy

Exploiting the Raman solver, a brute force strategy has been implemented to optimize Raman pumps parameters. This is just a first optimization approach that, given some constraints and minimization criteria, allows to choose an optimum solution from the space of solutions generated by a set of ranges in which parameters can vary.

So, the brute force strategy is based on the generation of a certain space of solution in which the optimum one has to be found.
The algorithm which generates the space of solution is illustrated in fig. 3.13. Given all the lists of parameters containing all values that can be assumed by each of them, the associated iterator with all possible combinations of input parameters is generated.

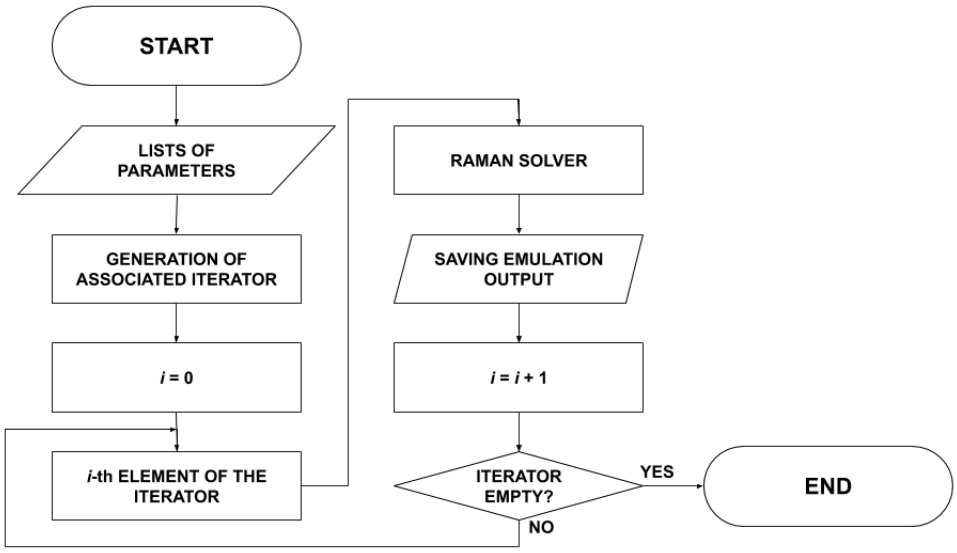

Figure 3.13: Solution space generator flow diagram.

Being the code developed in Python, an iterator is an object that contains a clusters' collection of objects of different nature, and can be scrolled to elaborate each of them in sequence. Starting from the lists with all parameters values, the associated iterator is built operating the Cartesian product over them. If lists are particularly dense of data, the use of iterators is extremely powerful due to the fact that they allows to save resources, being consumable objects. Furthermore, they avoid a heavy use of loops for the management of lists variables.
Once the iterator has been built, it is scrolled and at each iteration a set of input parameters is given to the Raman Solver and the solution is saved. At the end of the loop, when the iterator is consumed, the wanted space of solution is generated.

Starting from the solution space generator, a brute force approach has been implemented choosing properly what parameters have to be varied and their ranges and determining a metrics that allows to identify with suitable criteria the optimum solution.
The general algorithm is schematized in figure 3.14.
In the analysis carried out, the following parameters are taken into account to generate the lists which feed the solution space generator:

- Input power per channel level P_s;
- Spectrum grid (C band or C+L band);
- Input power of each Raman pump P_p.

For the spectrum grid, the space of solutions can range over both C and C+L configurations, considering solutions that belong to the same scenario but originate from different input signal pattern.
For the other parameters, the introduction of some constraints becomes necessary to fix bounds of ranges and the degree of granularity of the solution space. Optimization brute force strategies are very effective and simple but, if observation limits are not well calibrated and defined, the procedure becomes extremely time consuming and

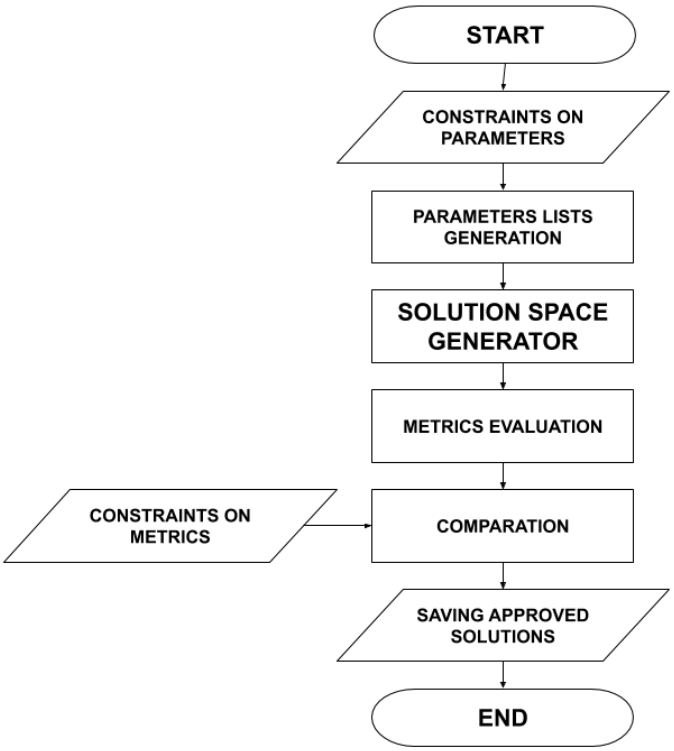

Figure 3.14: Brute force approach flow diagram.

heavy from a storage point of view. So, it is fundamental the choice of extremes of power variables and the number of steps in which these variables are discretized.
After having generated the solution space, each solution is elaborated in order to produce a metrics that allows to distinguish a bunch of them or the optimum one in base on optimization purposes. The adopted metrics will be properly described in the next subsection.
Applying some constraints on the metrics and making the comparison, approved solutions are selected and stored.

3.4.1 Metrics for brute force optimization

Considering Stimulated and Spontaneous Raman Scattering matrices of a single solution and focusing on power levels at the end of the fiber ($z = L_{span}$), on-off gain and noise figure profiles are derived and they become object of a further elaboration.

The metrics is computed distinguishing between C band and C+L band cases:

- **C band scenario**: the computation is operated over the entire spectrum;
  - C band only.
- **C+L band scenario**: the computation is operated dividing it into C band and L band.
  - C band, in C+L band scenario;
  - L band, in C+L band scenario.

This choice allows to have a better control and a higher number of degrees of freedom on the selection of the optimum solution.

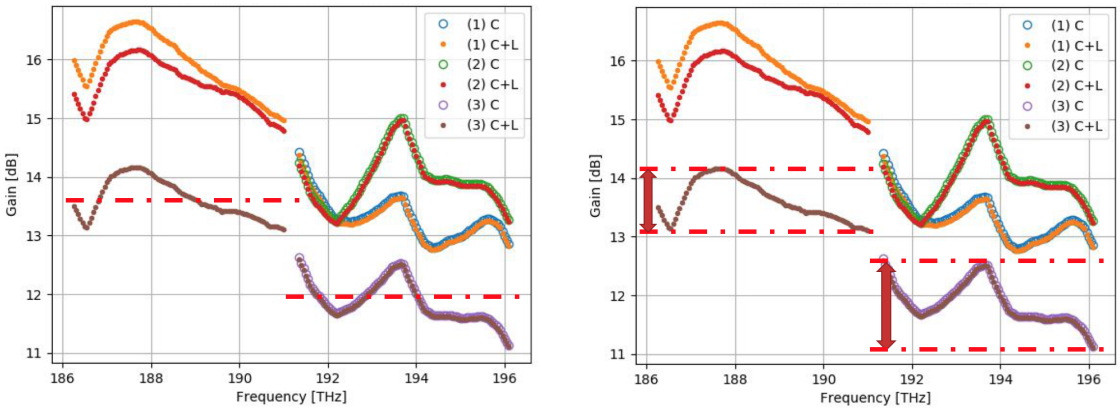

Figure 3.15: Graphic representation of the computation of average and ripple.

Starting from on-off gain and noise figure profiles, the average value and the maximum ripple are evaluated exploiting the following formulas:

$$\overline{a} = \frac{1}{n}\sum_{i=1}^{n} a(f_i)$$

$$\Delta a = max(a(f)) - min(a(f))$$

where a is the on-off gain G_{OO} or the noise figure NF, n is the number of channels, and f_i is the central frequency of the relative channel. All average and ripple computation are performed with quantities in dB.

In this way, the following list of metrics parameters is computed according to the input spectrum grid:

- **C band scenario**:
  - Average on-off gain $\overline{G_{OO}}(f_{Conly})$
  - Ripple on-off gain $\Delta G_{OO}(f_{Conly})$
  - Average noise figure $\overline{NF}(f_{Conly})$
  - Ripple noise figure $\Delta NF(f_{Conly})$
- **C+L band scenario**:
  - Average on-off gain in C band $\overline{G_{OO}}(f_C)$
  - Ripple on-off gain in C band $\Delta G_{OO}(f_C)$
  - Average noise figure in C band $\overline{NF}(f_C)$
  - Ripple noise figure in C band $\Delta NF(f_C)$
  - Average on-off gain in L band $\overline{G_{OO}}(f_L)$

– Ripple on-off gain in L band $\Delta G_{OO}(f_L)$
– Average noise figure in L band $\overline{NF}(f_L)$
– Ripple noise figure in L band $\Delta NF(f_L)$

Meanings of average operation and maximum ripple meaning are reported graphically in figure 3.15 over an example profile of on-off gain.

Constraints and minimization criteria are applied on the just described metrics, firstly selecting a group of solutions from the whole solution space fixing threshold values, for example:

$$\overline{G}_{OO}(f_C) > \overline{G}_{OO,target}(f_C)$$

$$\Delta NF(f_L) < \Delta NF_{target}(f_L)$$

and then establishing an optimization condition to selected the optimum scenario, for example:

$$min(\Delta NF(f_{Conly})).$$

3.5 Numerical optimization

In this section, the optimization problem has been addressed implementing a numerical optimizer which exploits an algorithm based on gradient method.
The entire framework is built on a numerical optimizer described within a SciPy [6] library package called *scipy.optimize* . This Python package provides many minimization algorithms to solve optimization problems.
In this case, the problem to solve regards a constrained multi-variable nonlinear function. The minimization method used for this purpose is the Sequential Least Squares Programming algorithm (SLSQP). It is adopted for problems which assume the following form:

$$\min_x f(x)$$

subject to:

$$c(x) = 0$$

$$c(x) \geq 0$$

$$lb_i \geq x_i \geq ub_i$$

where $f(x)$ is the object function, $c(x)$ is the set of equality or inequality constraints and lb_i and ub_i are bounds of the i-th variable to optimize.

The complete optimization algorithm is reported in figure 3.16.
The description of the problem is provided to the numerical optimizer through the following information:

- Constraints $c(x)$ (equalities or inequalities);
- Bounds for each variable to optimize lb_i, ub_i;
- Object function $f(x)$;
- Set of initial values x_0;

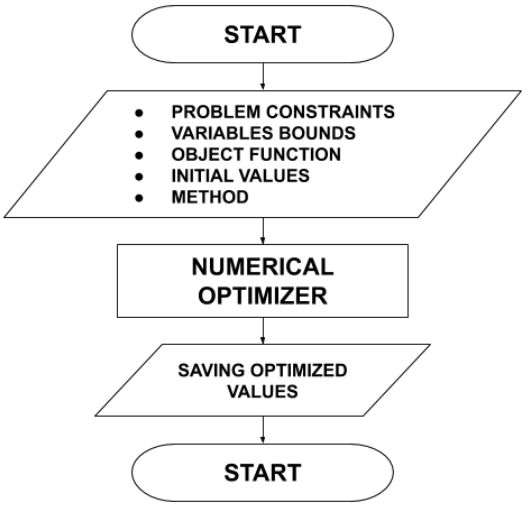

Figure 3.16: Optimization flow diagram.

- Method (SLSQP).

The use of the object function $f(x)$ and the set of initial values x_0 will be discussed in the next dedicated subsection.
During the research activity, three different optimization problem were defined.
The first two are respectively 4 and 5 variables optimization problems, where each Raman pump input power (one pump for each variable) is optimized, maintaining fixed all wavelengths.
The second one is a 10 variables in which both input powers and wavelengths of 5 Raman pumps are optimized.
Due to practical limits related to the implementation of likely real systems, the following constraints and bounds are imposed:

- **4 variables problem**:
  - **Bounds on pumps powers**: $500\,mW \geq P_{p,i} \geq 0, \quad i = 1, ..., 4$
  - **Constraint on maximum total pumps power**: $\sum_{i=1}^{4} P_{p,i} = 1.2\,W$
- **5 variables problem**:
  - **Bounds on pumps powers**: $500\,mW \geq P_{p,i} \geq 0, \quad i = 1, ..., 5$
  - **Constraint on maximum total pumps power**: $\sum_{i=1}^{5} P_{p,i} = 1.2\,W$
- **10 variables problem**:
  - **Bounds on pumps powers**: $(P_{p,i} + 25\,mW) \geq P_{p,i} \geq (P_{p,i} - 25\,mW)$, $i = 1, ..., 5$
  - **Bounds on pumps wavelengths**: $(\lambda_{p,i} + 3\,nm) \geq \lambda_{p,i} \geq (\lambda_{p,i} - 3\,nm)$, $i = 1, ..., 5$
  - **Constraint on maximum total pumps power**: $\sum_{i=1}^{5} P_{p,i} = 1.2\,W$

After having fed the numerical optimizer with the required parameters, the iterative algorithm tries to minimize the object function exploring the multidimensional space

of the solution and operating gradient evaluations.
When the tolerance is reached, the optimizer achieves the convergence and stops the optimization process providing the optimized configuration of input variables.

3.5.1 Object function

Also called loss function or cost function, the object function is a fundamental element of the framework and the question that the optimizer has to answer: to find the input configuration that minimizes it.

The general structure of the object function is reported in figure 3.17.
At the beginning, a set of variables to optimize is provided to the Raman solver, which computes the relative output. All the other parameters that are not subject to optimization process are fixed in advance.
From Raman Solver output, on-off gain profile is derived and the computation of its average value $\overline{G}_{OO}$ and maximum ripple ΔG_{OO} along the whole spectrum are computed, both for C band and C+L cases.
In the research activity, two final forms of the object function were adopted in different cases:

$$f(x) = \frac{\Delta G_{OO}}{\overline{G_{OO}}} \tag{3.3}$$

$$f(x) = \Delta G_{OO} + \mid \overline{G_{OO}} - \overline{G_{OO,target}} \mid \tag{3.4}$$

where $\overline{G_{OO,target}}$ is a target on-off gain value to achieve.

Considering the expression 3.3, it is constituted by a single term that is the ratio

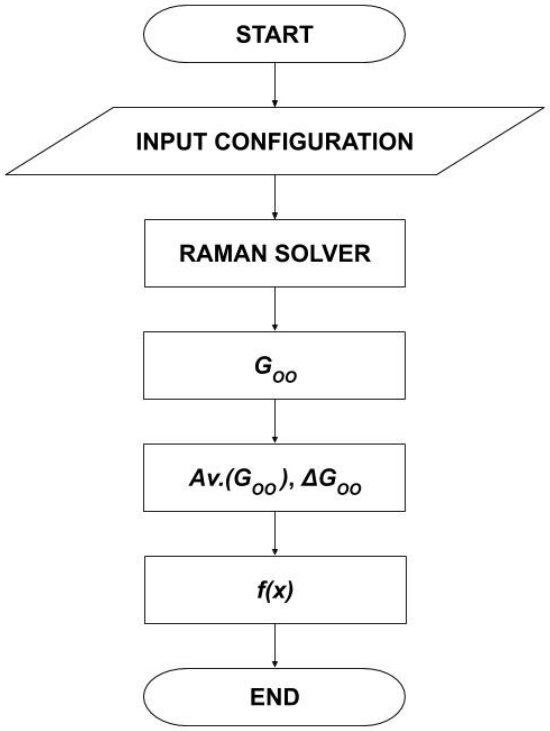

Figure 3.17: Object function flow diagram.

between the on-off gain ripple and its average value. The meaning of this expression is related to the will to obtain an on-off gain profile as flat as possible with the highest average value.
On the other hand, the expression 3.4 contains two terms. The first one is the on-off gain ripple, that the optimizer tries to minimize, and the second one is the absolute value of two average on-off gain values. The absolute value is needed to maintain the object function positive, while the ripple is positive by definition. Thanks to this form, the optimizer tries to cancel the second term, reaching the wanted target value, and to obtain the on-off gain mask with the minimum height.

The initial set of input values x_0 is fundamental for the success of the optimization result because it affects both the optimization time and the optimum configuration itself, if the problem presents local minima. For this reason, the investigation of the optimum solution is carried out executing more than one optimization, starting from different initial sets of variables to optimize. This kind of approach allows also to verify if the optimization problem has a convex nature, with a global minimum.

3.6 Sensitivities' evaluation

After having identified the optimum solution, a perturbation is applied on it and the analysis is carried out trying to understand how performances change if the working point of the system is moved around the optimum in the multidimensional space of the solution.

The complete algorithm is illustrated in figure 3.18.

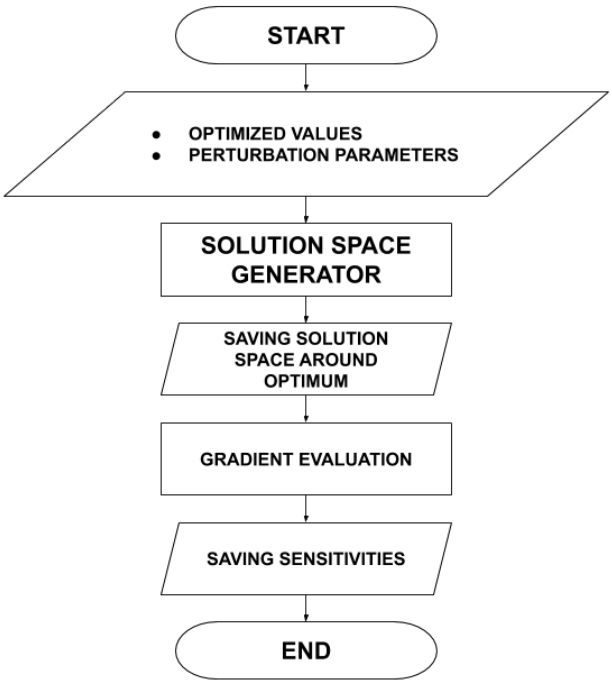

Figure 3.18: Sensitivities evaluation flow diagram.

Starting from the optimum solution, it is perturbed through some parameters for

the determination of the variation entity. In this way, parameters lists are generated and then are provided to the solution space generator.
Now, the overview of the possible behaviours around the optimum is obtained and each perturbed solution is submitted to a gradient evaluation with respect to the optimum one, in order to establish how much the system is affected by the variation of the interested parameter.

Perturbation is applied according to two different computations for sensitivity evaluation during the research.
The first one expresses the perturbation through a percentage and so the working point changes in base on a relative variation of the optimized parameter.
The second procedure moves the optimum solution in the solution space through an absolute variation, having a perturbation that does not depend on the entity of the optimized parameter.
In the following, a couple of examples explain how parameters lists are generated in order to properly obtain the behaviour of the working point around the optimum solution.

```
Example 1: Relative Sensitivity

    min_f = f(pp1_opt, pp2_opt, pp3_opt, pp4_opt, pp5_opt)
    perc = 0.1  # 10%

    var1 = pp1_opt * perc  # [W]
    aroundopt_pp1_up = f(pp1_opt+var1, pp2_opt, pp3_opt, pp4_opt, pp5_opt)
    aroundopt_pp1_down = f(pp1_opt-var1, pp2_opt, pp3_opt, pp4_opt, pp5_opt)

Example 2: Absolute Sensitivity

    min_f = f(pp1_opt, pp2_opt, pp3_opt, pp4_opt, pp5_opt)
    var = 1  # [nm]

    aroundopt_lp1_up = f(lp1+var, lp2, lp3, lp4, lp5)
    aroundopt_lp1_down = f(lp1-var, lp2, lp3, lp4, lp5)
```

Each couple of solutions have to be carried out for every pump, producing a set of 10 solutions around the optimum one, found optimizing 5 input variables.
To make easy the comprehension of the notation, the affix "UP" denotes an augmentation of the input variable with respect to the optimum one and, viceversa, the affix "DOWN" indicates a decrease of the input variable with respect to the optimum one.

In the results development, sensitivities with respect to pumps input powers are evaluated using relative variations, expressing their entities according to the following formulae:

$$S^{\overline{G_{OO}}}_{ppx_{\pm}} = \left| \frac{d\overline{G_{OO}}}{dppx_{\pm}} \right| = \left| \frac{\overline{G_{OO,opt}} - \overline{G_{OO,opt\pm varx}}}{10\log(1 \pm perc)} \right| \qquad [\frac{dB}{dB}]$$

$$S^{\Delta G_{OO}}_{ppx_{\pm}} = \left| \frac{d\Delta G_{OO}}{dppx_{\pm}} \right| = \left| \frac{\Delta G_{OO,opt} - \Delta G_{OO,opt\pm varx}}{10\log(1 \pm perc)} \right| \qquad [\frac{dB}{dB}]$$

where ppx is the pump power that undergoes the variation, $varx$ means the variation applied to the relative pump power and $\pm$ diversifies positive variations from negative variations.
Moreover, sensitivities with respect to pumps wavelengths are evaluated using absolute variations, expressing them through the following formulae:

$$S_{\lambda px_{\pm}}^{\overline{G_{OO}}} = \left| \frac{d\overline{G_{OO}}}{d\lambda px_{\pm}} \right| = \left| \frac{\overline{G_{OO,opt}} - \overline{G_{OO,opt\pm varx}}}{\pm var} \right| \qquad [\frac{dB}{nm}]$$

$$S_{\lambda px_{\pm}}^{\Delta G_{OO}} = \left| \frac{d\Delta G_{OO}}{d\lambda px_{\pm}} \right| = \left| \frac{\Delta G_{OO,opt} - \Delta G_{OO,opt\pm varx}}{\pm var} \right| \qquad [\frac{dB}{nm}]$$

where λpx is the pump wavelength that undergoes the variation, $varx$ means the variation applied to the relative pump wavelength and $\pm$ diversifies positive variations from negative variations.

Power sensitivities are been computed starting from the following percentages:

- $\pm$ 1%
- $\pm$ 5%
- $\pm$ 10%

Adopting these values, it is possible to evaluate performance changes within the typical variation range of Raman pumps.

For wavelength sensitivities, the following absolute variation are been chosen:

- $\pm$ 1 nm
- $\pm$ 2 nm
- $\pm$ 3 nm

Also in this case, laser gratings allow to obtain a deviation from the nominal wavelength of the Raman pump of a few nanometers.

Chapter 4

Results

After having explained all methodologies adopted during the research activity, derived results are illustrated and analyzed in this chapter.
The work-flow of the study was led initially by preliminary goals and then by intermediate outcomes, focusing the discussion of performance mainly on the on-off gain profile characteristics.

On the basis of procedures described in the previous chapter, the analysis of the results is carried out firstly outlining the scenario and explaining how the methodology is used, then showing the relative outcome throughout the support of graphs and tables.

4.1 Brute forces strategy - 4 Raman pumps

At the beginning of the investigation on Raman amplification, the first approach that was adopted to understand characteristics of input Raman pumps' configuration was a brute force strategy.
Generating the solution space and analysing metrics, it was possible to have a general comprehension of the phenomenon in multi-pump scenario and a more immediate perception of how modifications of the input configuration affect the output on-off gain and noise figure profiles.

The scenario under analysis presents the following features:

- Fiber link length: 120 km;
- 4 counter-propagating Raman pumps;
- Set of Raman pumps' wavelengths (fixed):
  - 1425 nm
  - 1440 nm
  - 1458 nm
  - 1495 nm

The solution space of this scenario is generated by all possible combination of the following parameters:

- Input power per channel level P_s:
  - -10 dBm
  - 0 dBm
- Spectrum grid (spacing of 50 GHz among adjacent channels):
  - C band: 96 channels
  - C+L band: 192 channels (96 + 96)
- Input power of each Raman pump P_p:
  - 0 mW
  - 125 mW
  - 250 mW
  - 375 mW
  - 500 mW

Once the solution space is created, for each emulation relative metrics is computed to estimate the quality of the amplification.
Then constraints on average and ripple values are imposed in order to select from emulations a subset of scenarios with peculiar features. In particular, the following margins are established:

$$\Delta G_{OO}(f_{Conly}) < 1.65\,dB \quad and \quad \Delta G_{OO}(f_C) < 1.65\,dB \quad and \quad \Delta G_{OO}(f_L) < 1.65\,dB$$

$$\overline{G_{OO}}(f_{Conly}) > 10\,dB \quad and \quad \overline{G_{OO}}(f_C) > 10\,dB \quad and \quad \overline{G_{OO}}(f_L) > 10\,dB$$

Those limits are imposed on each couple of C/C+L scenarios on average and ripple values in order to find a Raman pumps configuration capable to reach at least a certain gain level with a restricted ripple in both C and C+L cases.

Imposing constraints on computing metrics, the cases reported in figure 4.1 match the required features.

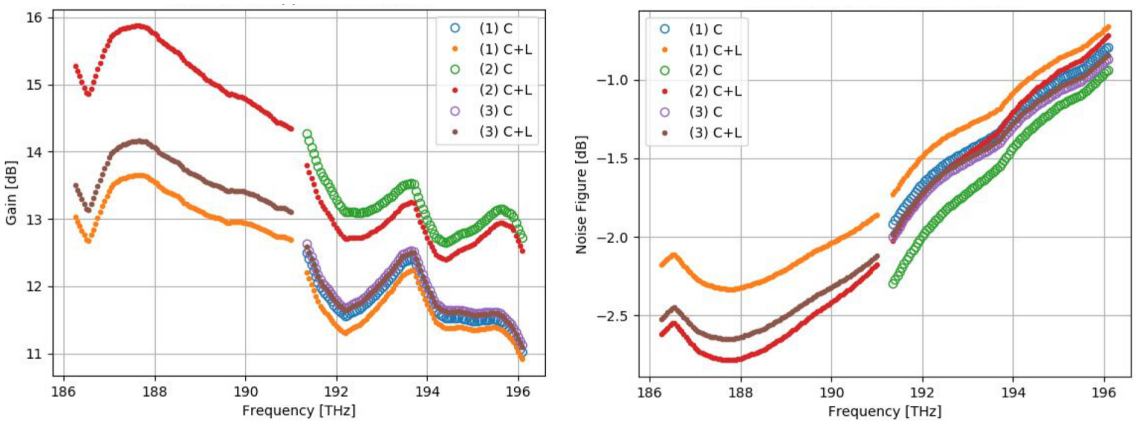

Figure 4.1: Brute force strategy - gain and noise figure profiles of selected scenarios.

In table 4.1 are reported input configurations that generate the approved double

N Scenario	Power per channel [dBm]	Power pump 1 [mW]	Power pump 2 [mW]	Power pump 3 [mW]	Power pump 4 [mW]
1)	0	125	250	125	250
2)	0	250	250	125	250
3)	-10	125	250	125	250

Table 4.1: Configurations of the selected scenarios considering metrics constraints.

N Scenario	$\overline{G_{OO}}(f_C)$ [dB]	$\overline{G_{OO}}(f_L)$ [dB]	$\overline{G_{OO}}(f_{Conly})$ [dB]	$\Delta G_{OO}(f_C)$ [dB]	$\Delta G_{OO}(f_L)$ [dB]	$\Delta G_{OO}(f_{Conly})$ [dB]
1)	11.57	13.14	11.75	1.32	0.97	1.48
2)	12.85	15.18	13.15	1.39	1.53	1.62
3)	11.84	13.62	11.87	1.48	1.05	1.49

Table 4.2: Metrics of the selected scenarios - on-off gain metrics.

N Scenario	$\overline{NF}(f_C)$ [dB]	$\overline{NF}(f_L)$ [dB]	$\overline{NF}(f_{Conly})$ [dB]	$\Delta NF(f_C)$ [dB]	$\Delta NF(f_L)$ [dB]	$\Delta NF(f_{Conly})$ [dB]
1)	-1.14	-2.16	-1.29	1.06	0.47	1.12
2)	-1.29	-2.57	-1.53	1.30	0.61	1.35
3)	-1.34	-2.46	-1.37	1.13	0.53	1.13

Table 4.3: Metrics of the selected scenarios - noise figure metrics.

scenarios C/C+L that match constraints, and in tables 4.2 and 4.3 are present the relative metrics computed.

Observing on-off gain profiles and relative metrics, it is remarkable the fact that, turning on and off L band in the C+L scenario, the relative C band one does not change sensibly performance. The slight variation is more evident for cases when a higher input power per channel level (0 dBm) is introduced. This is due to pump depletion and inter-channel Raman effect, because the turning off of the L band avoids further power transfer over C band frequencies. So, in C band scenarios, the relative on-off gain profile is slightly higher than the corresponding C+L scenario.

The brute force strategy adopted is just a first approach to the problem.
It shows some intrinsic difficulties in the use for the achievement of the goals related mainly to the granularity of the solution space. This one is directly proportional to the time needed to generate the solution space and to storage resources, but brute force approach is effective only if the discretization of the solution space is high, and so time consumption is the main issue that does not allow enough flexibility for Raman amplifiers design in case of modifications of the scenario under analysis.

4.2 First optimization approach - 4 Raman pumps

A first kind of numerical optimization approach has been carried out in order to improve the control on the selection of the final input configuration and to reduce time consumption.

In the optimization method, only input constraints are considered. In order to focus the optimizer on a solution that minimizes on-off gain ripple and maximizes

the on-off gain average value, initially, the objective function $f(x)$ has been written following the expression 3.3.
For convenience, the description of the scenario to optimize is reported in the following:

- Fiber link length $L_{span} = 120\,km$;
- C band grid (96 channels);
- Input power per channel $P_s = -10\,dBm$;
- 4 counter-propagating Raman pumps;
- Set of Raman pumps' wavelengths (fixed):
  - 1425 nm
  - 1440 nm
  - 1458 nm
  - 1495 nm
- **4 variables problem**:
  - **Bounds on pumps powers**: $500\,mW \geq P_{p,i} \geq 0, \quad i = 1, ..., 4$
  - **Constraint on maximum total pumps power**: $\sum_{i=1}^{4} P_{p,i} = 1.2\,W$
  - **Object function**: $f(x) = \frac{\Delta G_{OO}}{G_{OO}}$

In order to test the numerical optimizer and to observe the appearance of the objective function $f(x)$, more than one optimization was performed starting from different sets of initial values x_0 which are contained in table 4.4.

Initial values			
Power pump 1 [mW]	**Power pump 2 [mW]**	**Power pump 3 [mW]**	**Power pump 4 [mW]**
50	50	50	50
100	100	100	100
250	250	250	250
290	290	290	290

Table 4.4: Sets of initial values for optimization, 4 Raman pumps, C band.

From these sets of initial values x_0, four problem optimizations were performed and the optimized input power configurations are reported in table 4.5.
Just observing the final optimized values, it is remarkable the fact that only the first two optimization present a similar configuration of pumps' input powers, while the others are completely different. From this, it is possible to affirm that the optimized objective function shows more than one minimum, and so the final result of the optimization procedure depends on the initial set of values.

Running the Raman solver with final sets of pumps input power configuration,

Final input configurations			
Power pump 1 [mW]	**Power pump 2 [mW]**	**Power pump 3 [mW]**	**Power pump 4 [mW]**
138	53	231	68
148	48	251	60
334	97	411	56
483	132	497	46

Table 4.5: Sets of optimized input configurations, 4 Raman pumps, C band.

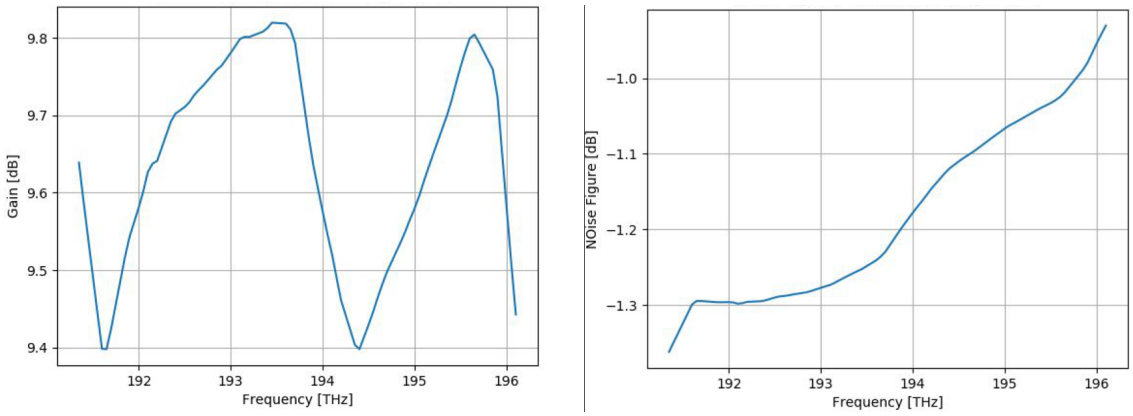

Figure 4.2: Optimization - gain and noise figure profiles, 4 Raman pumps, C band - scenario 1.

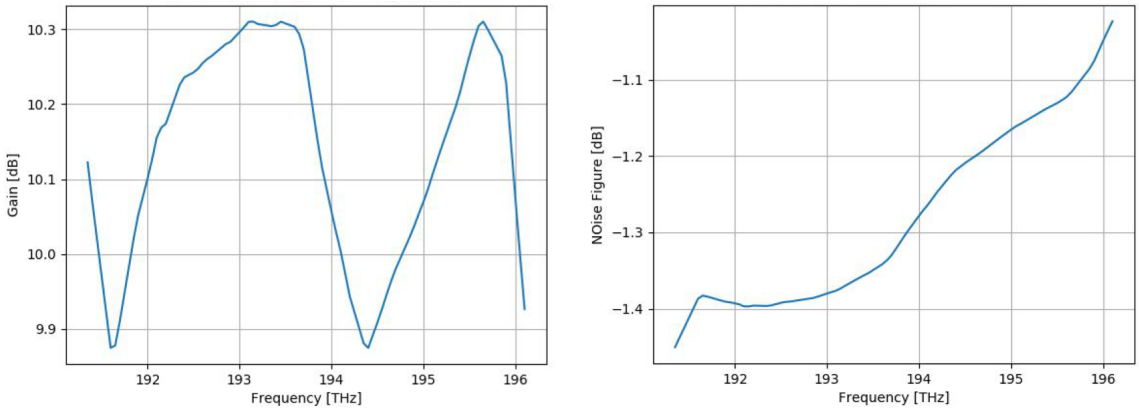

Figure 4.3: Optimization - gain and noise figure profiles, 4 Raman pumps, C band - scenario 2.

optimized on-off gain and noise figure profiles are obtained. In figures 4.2, 4.3, 4.4, 4.5 the corresponding curves are reported.
For each on-off gain profile, the relative metrics is computed and results are resumed in table 4.6.

Even if each optimization has different average values and ripples, all curves present same shape. This is due probably to a property of the object function when is evaluated in a local minimum.
In the object function, as described, there is not any reference to possible targets to

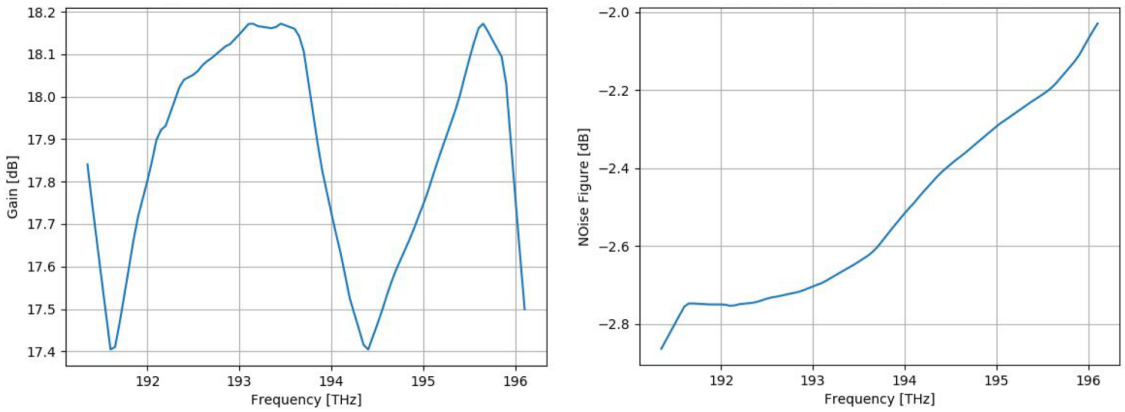

Figure 4.4: Optimization - gain and noise figure profiles, 4 Raman pumps, C band - scenario 3.

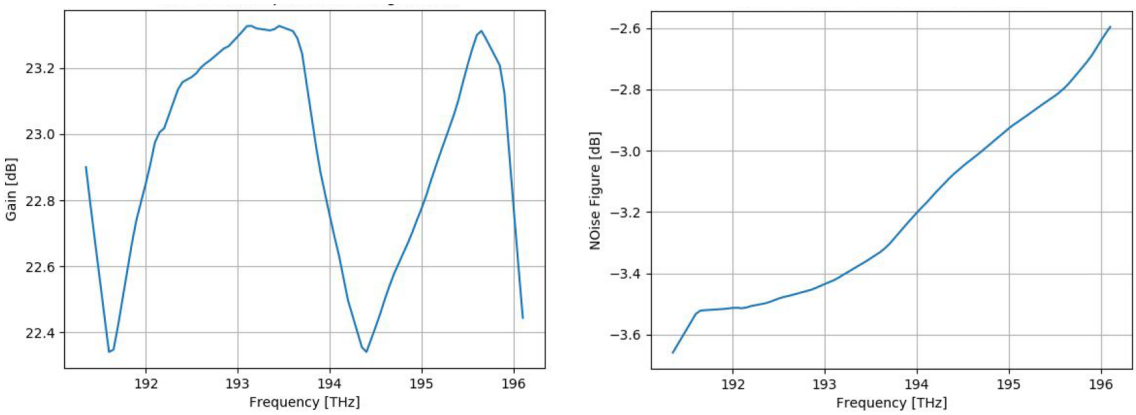

Figure 4.5: Optimization - gain and noise figure profiles, 4 Raman pumps, C band - scenario 4.

Metrics		
$\overline{G_{OO}}$ **[dB]**	ΔG_{OO} **[dB]**	**Function minimum [dB/dB]**
9.64	0.42	0.0438
10.13	0.44	0.0429
17.87	0.77	0.0429
22.93	0.99	0.0431

Table 4.6: Metrics of optimized input configurations, 4 Raman pumps, C band.

achieve in order to have control on output profiles characteristics. For this reason, the formulation used in the problem does not present a single minimum; this is due to the fact that in the object function expression the product of on-off average gain and ripple allows only to be minimized and not to be managed as if some output constraints were imposed.

4.3 New optimization formulation - 5 Raman pumps

Starting from the last question, the problem formulation has been changed in order to optimize pumps input power configuration achieving a target on-off average gain, trying to add the description of output constraints inside the expression of the object function.

The new object function proposed for the optimization of the problem is the expression 3.4. While the first term which coincides with the on-off gain ripple has to be minimize as much as possible, the second term contains the on-off average gain and, as its form suggests, it has to be cancelled by the numerical optimizer finding a configuration of input parameters that matches the target gain.

In order to improve the shape of the on-off gain profile, making it less twisty, and so to reduce the on-off gain ripple, the set of Raman pumps was incremented with the insertion of a fifth pump.
Being the entity of interaction among pumps and channels handled by the Raman efficiency curve of the fiber, which has not properly a straight and smooth trend, the use of a higher number of Raman pumps allows to have a more homogeneous amplification of channels power, without exceeding the maximum total pumps power.
This choice is also made in view of optimizing C+L band scenario where spectrum is considerably wide and the inclusion of a Raman pump that works at L band range helps to manage amplification of low-frequency channels.

The description of the scenario to optimize is reported in the following:

- Fiber link length $L_{span} = 120\,km$;
- C band grid (96 channels);
- Input power per channel $P_s = -10\,dBm$;
- 5 counter-propagating Raman pumps;
- Set of Raman pumps' wavelengths (fixed):
  - 1424 nm
  - 1438 nm
  - 1457 nm
  - 1470 nm
  - 1495 nm
- **5 variables problem**:
  - **Bounds on pumps powers**: $500\,mW \geq P_{p,i} \geq 0, \quad i = 1, ..., 5$
  - **Constraint on maximum total pumps power**: $\sum_{i=1}^{5} P_{p,i} = 1.2\,W$
  - **Object function**: $f(x) = \Delta G_{OO} + \mid \overline{G_{OO}} - \overline{G_{OO,target}} \mid$,
    with $\overline{G_{OO,target}} = 10\,dB$

where on-off average gain target $\overline{G_{OO,target}}$ is the on-off average gain requested by constraint.

Being the first optimization with this new problem formulation, the on-off average gain target is set at a not so high value for standards, in order to increment it in further analysis.
The optimization was carried out for 4 different sets of initial values, in order to observe if the object function presents one global minimum or more than one local minima.
The sets of initial values with which optimizations are performed are reported in table 4.7 and the optimized pumps input power configurations are shown in table 4.8.

Initial values				
Power pump 1 [mW]	**Power pump 2 [mW]**	**Power pump 3 [mW]**	**Power pump 4 [mW]**	**Power pump 5 [mW]**
50	50	50	50	50
100	100	100	100	100
150	150	150	150	150
200	200	200	200	200

Table 4.7: Sets of initial values for optimization, 5 Raman pumps, C band - target gain = 10 dB.

Final input configurations				
Power pump 1 [mW]	**Power pump 2 [mW]**	**Power pump 3 [mW]**	**Power pump 4 [mW]**	**Power pump 5 [mW]**
142	48	243	12	52
142	48	244	10	53
143	48	235	24	43
143	48	241	15	51

Table 4.8: Sets of optimized input configurations, 5 Raman pumps, C band - target gain = 10 dB.

In this case, optimized configurations practically coincide. So, the problem formulated as previously described seems to be a convex function of the input variables. In other words, for every set of initial values provided, the optimizer finds always the same optimized configuration of inputs because the function presents a single global minimum. Differences of power values among corresponding pumps are related to the tolerance of the optimizer.
From a design point of view, this property is very significant because it means that thanks to a single optimization it is possible to understand of which entity Raman pumps power have to be set in order to achieve the request performance.

For each optimized configuration, relative on-off gain and noise figure profiles are reported in figures 4.6, 4.7, 4.8 and 4.9.
As might be expected, from the graphs it is possible to declare that each optimized configuration outlines the same scenario.

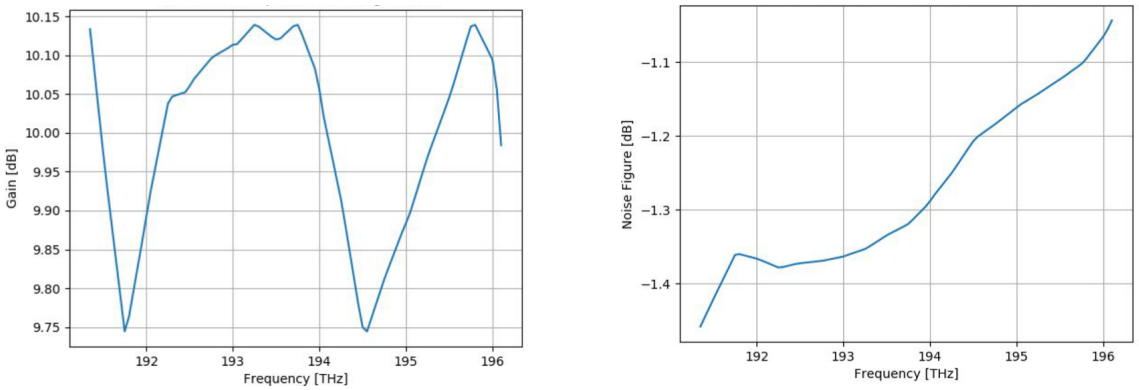

Figure 4.6: Optimization - gain and noise figure profiles, 5 Raman pumps, C band, target gain = 10 dB - scenario 1.

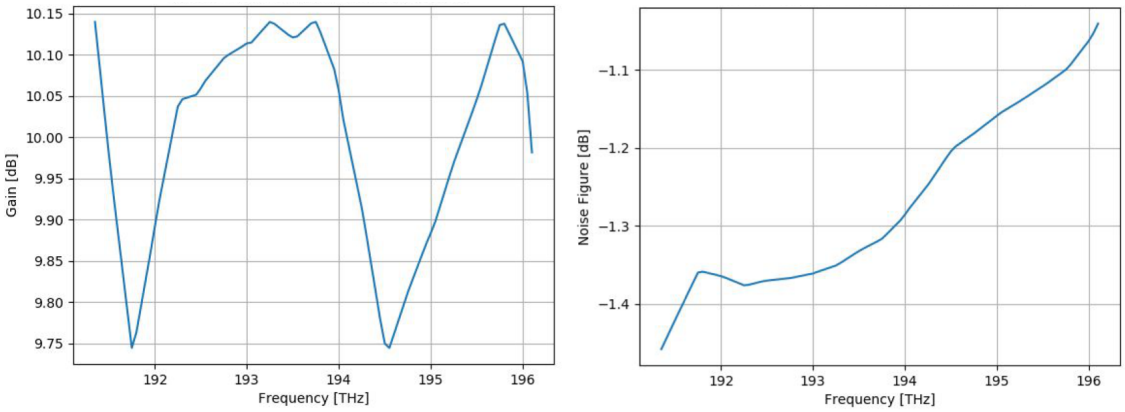

Figure 4.7: Optimization - gain and noise figure profiles, 5 Raman pumps, C band, target gain = 10 dB - scenario 2.

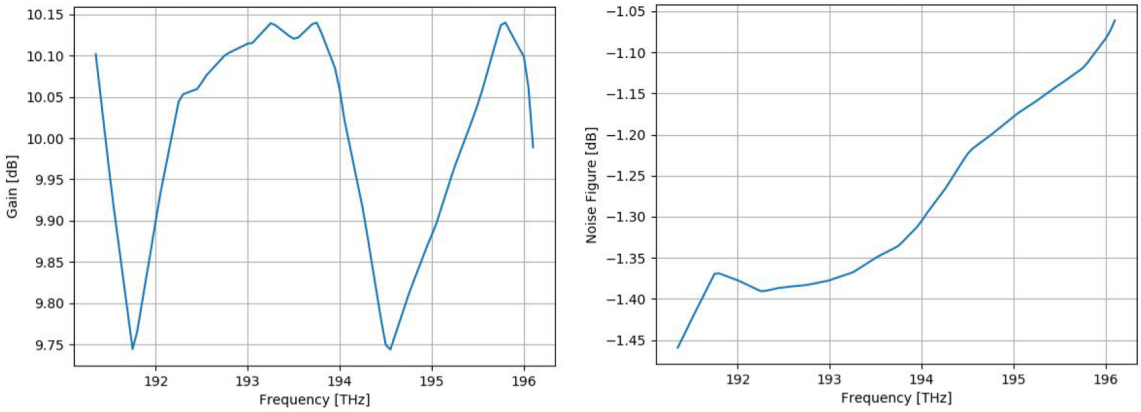

Figure 4.8: Optimization - gain and noise figure profiles, 5 Raman pumps, C band, target gain = 10 dB - scenario 3.

In table 4.9 all metrics related to each on-off gain profile is reported. From the derived data, it is clear the fact that the on-off average gain target has been fully centred by the optimizer and the entity of the on-off gain ripple is very small. This characteristic is so interesting from a communication point of view, because the spectrum undergoes an amplification as uniform as the on-off gain ripple is limited. So, for a C band spectrum, ripples under 0.5 dB can be considered quite reduced.

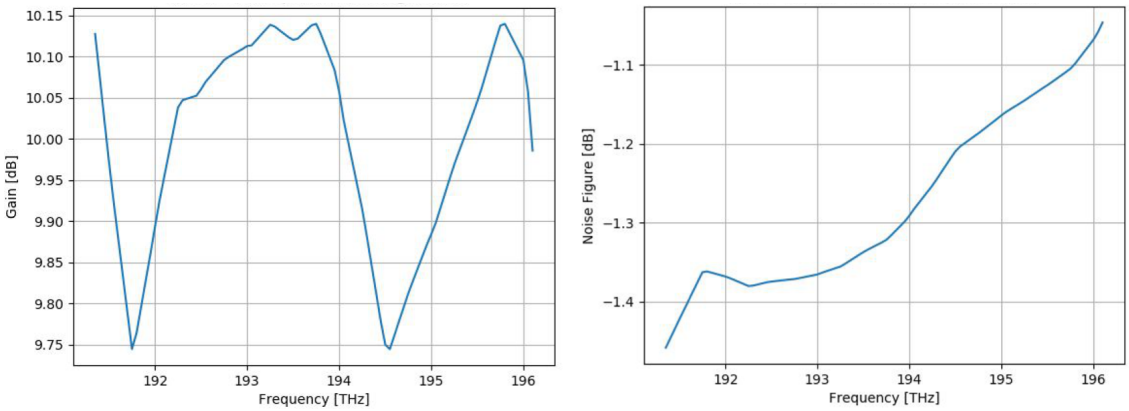

Figure 4.9: Optimization - gain and noise figure profiles, 5 Raman pumps, C band, target gain = 10 dB - scenario 4.

Metrics		
$\overline{G_{OO}}$ [dB]	ΔG_{OO} [dB]	**Function minimum [dB]**
10.00	0.394	0.395
9.99	0.395	0.395
9.99	0.396	0.396
9.99	0.395	0.395

Table 4.9: Metrics of optimized input configurations, 5 Raman pumps, C band - target gain = 10 dB.

4.3.1 Input powers sensitivity evaluation

Starting from the optimum solution, that seems to be unique in this case, sensitivities of performance metrics on-off average gain $\overline{G_{OO}}$ and on-off gain ripple ΔG_{OO} with respect to variations of each optimized input parameter are evaluated thanks to the computation of the gradient.

Thanks to the study of perturbed solutions around the optimum one, it is possible to understand if the function has a recognizable shape in the multi-dimensional space and how much the system is sensible to a possible variation of the considered input parameter.
In this case, the optimum solution was perturbed modifying each pump input power in percentage.

As previously described in the methodology, variations of 1%, 5% and 10% of each pump input power are applied to the optimum solution. In tables 4.10, 4.11 and 4.12 sensitivities and variations of the relative performance are reported.

Tables are vertically divided into two main parts: the first one is related to on-off average value and the second to the on-off gain ripple. On the other hand, the table also horizontally divided into three parts. The central one is dedicated

to optimum solution metrics and the other two are sensitivities and metrics of the perturbed solutions. "UP" and "DOWN" differentiate positive perturbations from negative perturbations applied to the optimum solution and for each of them the computed gradient and the value of the performance is reported.

Var = 1%	Average On-Off Gain					Ripple On-Off Gain					
	pp1	**pp2**	**pp3**	**pp4**	**pp5**	**pp1**	**pp2**	**pp3**	**pp4**	**pp5**	
	0.439	0.220	1.489	0.064	0.059	0.296	0.157	0.195	0.017	0.093	**Gradient [dB/dB]**
UP	10.018	10.010	10.064	10.003	10.002	0.408	0.397	0.403	0.396	0.399	**Value [dB]**
OPTIMUM	*10.000*					*0.395*					**[dB]**
	9.981	9.990	9.936	9.997	9.997	0.397	0.401	0.414	0.397	0.406	**Value [dB]**
DOWN	0.435	0.218	1.475	0.063	0.059	0.041	0.053	0.430	0.052	0.250	**Gradient [dB/dB]**

Table 4.10: Overview of the perturbation around the optimum solution - target gain = 10 dB, C band, Variation = 1%.

Var = 5%	Average On-Off Gain					Ripple On-Off Gain					
	pp1	**pp2**	**pp3**	**pp4**	**pp5**	**pp1**	**pp2**	**pp3**	**pp4**	**pp5**	
	0.448	0.225	1.517	0.065	0.061	0.303	0.161	0.207	0.018	0.201	**Gradient [dB/dB]**
UP	10.095	10.048	10.321	10.014	10.012	0.459	0.429	0.439	0.398	0.437	**Value [dB]**
OPTIMUM	*10.000*					*0.395*					**[dB]**
	9.905	9.952	9.678	9.986	9.987	0.404	0.423	0.489	0.406	0.450	**Value [dB]**
DOWN	0.426	0.214	1.446	0.062	0.057	0.041	0.126	0.425	0.054	0.248	**Gradient [dB/dB]**

Table 4.11: Overview of the perturbation around the optimum solution - target gain = 10 dB, C band, Variation = 5%.

Var = 10%	Average On-Off Gain					Ripple On-Off Gain					
	pp1	**pp2**	**pp3**	**pp4**	**pp5**	**pp1**	**pp2**	**pp3**	**pp4**	**pp5**	
	0.459	0.230	1.552	0.067	0.063	0.310	0.164	0.225	0.024	0.218	**Gradient [dB/dB]**
UP	10.190	10.095	10.642	10.028	10.026	0.523	0.463	0.488	0.404	0.485	**Value [dB]**
OPTIMUM	*10.000*					*0.395*					**[dB]**
	9.810	9.905	9.355	9.972	9.975	0.412	0.456	0.585	0.418	0.506	**Value [dB]**
DOWN	0.415	0.208	1.410	0.060	0.055	0.039	0.135	0.415	0.053	0.243	**Gradient [dB/dB]**

Table 4.12: Overview of the perturbation around the optimum solution - target gain = 10 dB, C band, Variation = 10%.

The unit of measure of the gradient is dB/dB. This choice allows to have easily an idea of the variation of the performance if a perturbation of 1 dB of the a pump input power is applied to the system.

From a first observation, it is possible to assert that Raman pumps placed at higher

frequency (lower wavelength) have a stronger impact on system performances, for both on-off average gain and on-off gain ripple. This is quite reasonable, because they have the highest interaction with the C band spectrum due to the peaks position in the Raman efficiency curve.
Analysing and comparing gradients obtained using different percentages of variation, it is remarkable the fact that they are practically symmetric with respect to the perturbation sign for on-off average gain and their values do not change significantly even increasing the entity of the variation. This means that, starting from the optimum solution, the multi-dimensional space is almost linear along a single dimension. Linearizing the function in an interval close to the minimum, it is possible to describe the variation of performances due to the variation of one input parameter thanks to a single number.
This kind of information is very important in order to understand which Raman pump has to be more stable in the configuration to not degrade performance.

4.4 Optimization for higher gain level - 5 Raman pumps

At this point, the potentiality of the new formulation has been proved. In addition to the fact that the problem seems to have an aptitude favourable to be optimized, in the previous analysis it has been observed the convexity of the object function for the performed optimizations and the possibility to linearize the multi-dimensional space of the solution along a single dimension close to the minimum.
From a mathematical point of view, this result is relevant and very attractive because of the simplicity and the shape of the solution starting from a set of ordinary differential equations.

Since in hybrid amplifiers, which exploit both distributed Raman amplification and EDFAs, Raman pumps configuration is generally designed to reach an on-off average gain as high as possible in order to not strain EDFAs and to achieve easily the required signal power level, in the following section the same optimization procedure has been performed of the previous one setting the on-off gain target $\overline{G_{OO,target}}$ equal to **16 dB**.
In general, when the amplifier gain increases, it undergoes saturation effects due to the stronger interaction among pumps and spectrum that determines the pumps depletion.

For sake of completeness, the description of the scenario to optimize is reported in the following:

- Fiber link length $L_{span} = 120\,km$;
- C band grid (96 channels);
- Input power per channel $P_s = -10\,dBm$;
- 5 counter-propagating Raman pumps;
- Set of Raman pumps' wavelengths (fixed):

  - 1424 nm
  - 1438 nm
  - 1457 nm
  - 1470 nm
  - 1495 nm

- **5 variables problem**:
  - **Bounds on pumps powers**: $500\,mW \geq P_{p,i} \geq 0, \quad i = 1, ..., 5$
  - **Constraint on maximum total pumps power**: $\sum_{i=1}^{5} P_{p,i} = 1.2\,W$
  - **Object function**: $f(x) = \Delta G_{OO} + \mid \overline{G_{OO}} - \overline{G_{OO,target}} \mid$, with $\overline{G_{OO,target}} = 16\,dB$

Treating a nonlinear problem, more than one optimization are performed in order to study the shape of the multi-variable function.
Sets of initial values used are reported in table 4.13.

Initial values				
Power pump 1 [mW]	**Power pump 2 [mW]**	**Power pump 3 [mW]**	**Power pump 4 [mW]**	**Power pump 5 [mW]**
50	50	50	50	50
100	100	100	100	100
150	150	150	150	150
200	200	200	200	200

Table 4.13: Sets of initial values for optimization, 5 Raman pumps, C band - target gain = 16 dB.

As result of optimizations, the final Raman pumps configurations found are reported in table 4.14.
Comparing powers of each Raman pump, the optimized input configurations are clearly not referred to a single solution, due to the evident difference among parameters values. This could be related to the fact that, increasing the on-off average gain target, the new function presents many local minima. Probably, there are more than one pumps configuration that allows to reach the on-off gain target maintaining the on-off gain ripple comparable with that of the other local minima.

For each optimization, the relative on-off gain and noise figure graphs are reported

Final input configurations				
Power pump 1 [mW]	**Power pump 2 [mW]**	**Power pump 3 [mW]**	**Power pump 4 [mW]**	**Power pump 5 [mW]**
286	89	308	76	32
293	164	283	27	88
284	111	347	18	64
278	87	351	33	43

Table 4.14: Sets of optimized input configurations, 5 Raman pumps, C band - target gain = 16 dB.

in figures 4.10, 4.11, 4.12 and 4.13.
The shapes of profiles are completely different among them. This confirms that many points of the multi-dimensional space are been evaluated. In general, it is possible to say that every on-off gain mask is placed around the on-off average gain target and each one of them has similar values of on-off gain ripple. As in the previous case, pumps with higher power values are placed at higher frequency because of their stronger interaction with C band spectrum, described through the Raman efficiency curve.

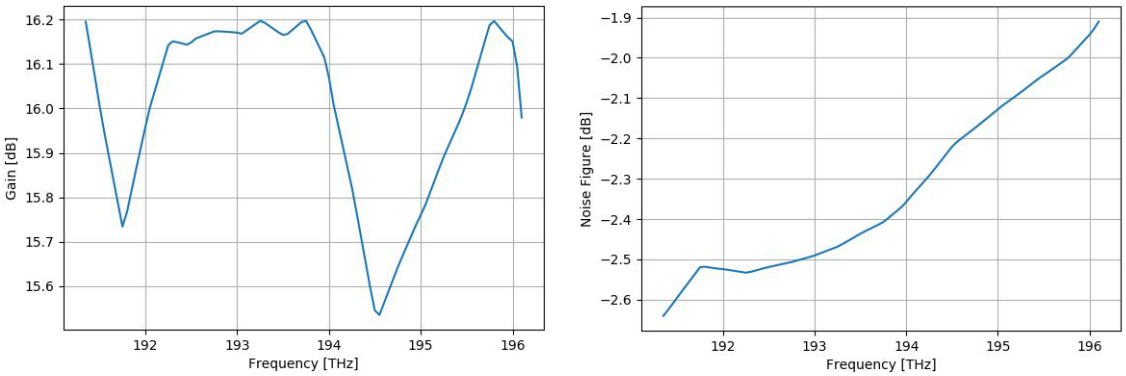

Figure 4.10: Optimization - gain and noise figure profiles, 5 Raman pumps, C band, target gain = 16 dB - scenario 1.

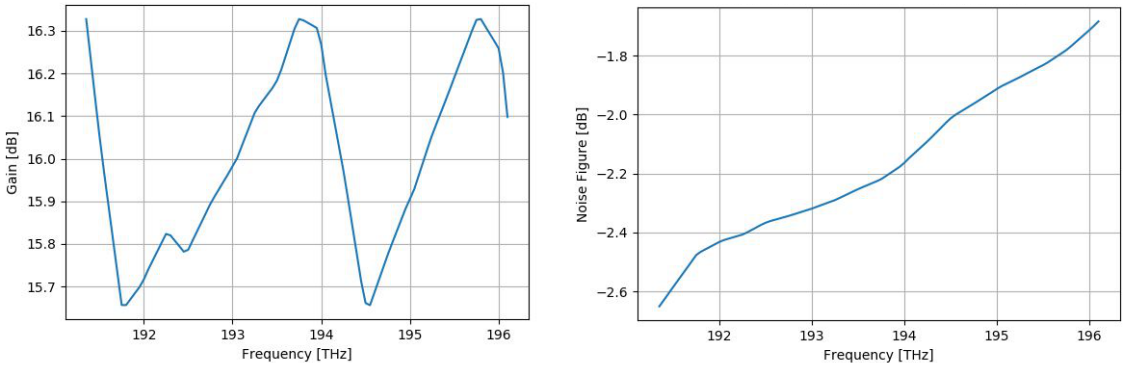

Figure 4.11: Optimization - gain and noise figure profiles, 5 Raman pumps, C band, target gain = 16 dB - scenario 2.

In table 4.15 are reported the relative metrics for each performed optimization.
In any case, the on-off average gain target has been achieved and the on-off gain ripple continues to have moderate values. Its value increases almost 0.25 dB more with respect to the previous case ($\overline{G_{OO,target}}$ =10 dB).
Even if each scenario is different from the others, performance parameters are extremely similar and so local minima have practically same nominal properties in the working point in terms of on-off gain. Also the maximum total pumps powers of each optimization are of the same entity that is around 800 mW.

From the analysis carried out, it has been shown that the optimizer works fine on the so described optimization problem, but from a mathematical point of view

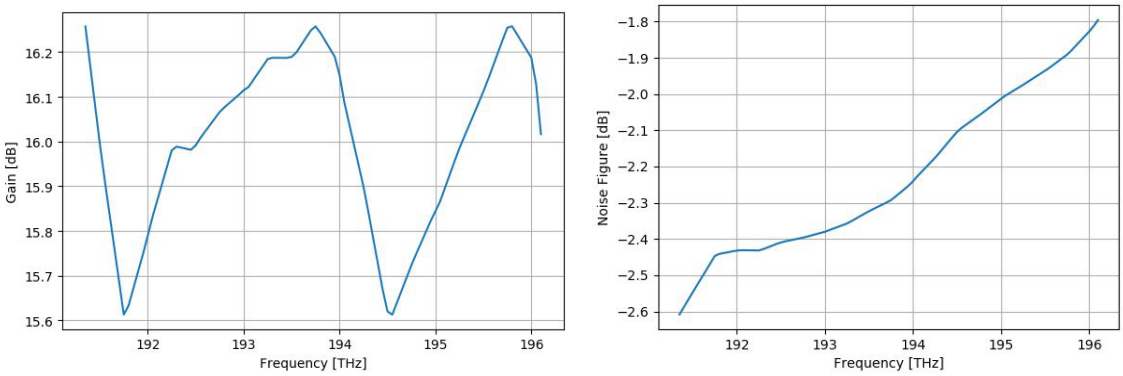

Figure 4.12: Optimization - gain and noise figure profiles, 5 Raman pumps, C band, target gain = 16 dB - scenario 3.

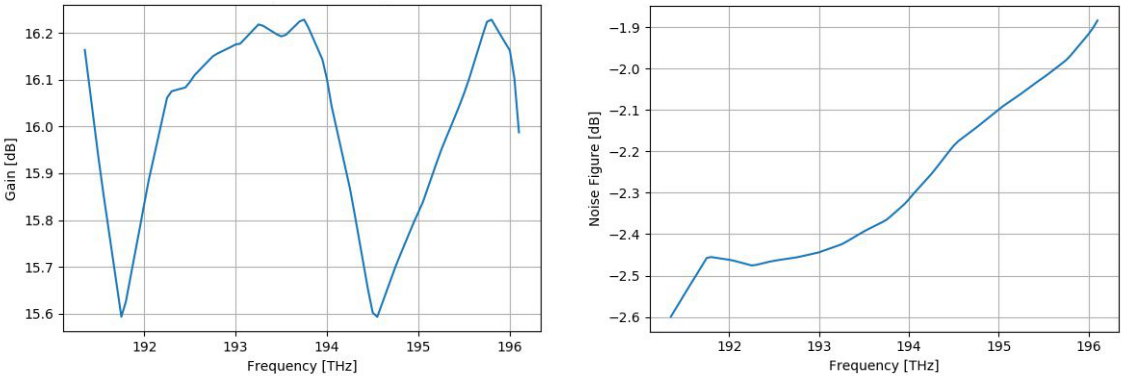

Figure 4.13: Optimization - gain and noise figure profiles, 5 Raman pumps, C band, target gain = 16 dB - scenario 4.

Metrics		
$\overline{G_{OO}}$ **[dB]**	ΔG_{OO} **[dB]**	**Function minimum [dB]**
15.999	0.663	0.663
16.000	0.671	0.671
15.999	0.645	0.645
15.999	0.636	0.636

Table 4.15: Metrics of optimized input configurations, 5 Raman pumps, C band, target gain = 16 dB.

the solution space has changed is shape due to the increasing of the on-off average gain target. The optimum solution is no more unique because from a condition of global minimum it has been passed to a function that presents more than one local minimum. Never the less, each optimized solution has performance characteristics which are very similar among them.

The change of the function morphology is probably due to the fact that, increasing the on-off average gain target, the second term of the objective function assumes a higher weight inside the expression, and so during the optimization procedure, the

definition of the local minimum is determine by the achievement of the target. This one is in its turn detected in base on the choice of the set of initial values. As last refinement step, the on-off gain ripple is minimized in the selected portion of the multi-dimensional solution space.

4.4.1 Input powers sensitivity evaluation

Even in this case, it is evaluated how the system modifies performances in response to a perturbation through the computation of the gradient of the solution with respect to input parameters variation.

Having more than one optimum, it is now considered the solution with has the lower function minimum. In this way, it is possible to say that the analysis is carried out on the actual global minimum computed.
For sake of clarity, the used optimum configuration of pumps is reported in the following:

- 1425 nm - $P_{p1,opt} = 278$ mW
- 1438 nm - $P_{p2,opt} = 87$ mW
- 1457 nm - $P_{p3,opt} = 351$ mW
- 1470 nm - $P_{p4,opt} = 33$ mW
- 1495 nm - $P_{p5,opt} = 43$ mW

Percentage variations relative to input power of each Raman pump are applied to the optimum solution. In tables 4.16, 4.17 and 4.18, all data of sensitivity and performance modifications are reported.

Var = 1%	Average On-Off Gain					Ripple On-Off Gain					
	pp1	**pp2**	**pp3**	**pp4**	**pp5**	**pp1**	**pp2**	**pp3**	**pp4**	**pp5**	
UP	0.902	0.401	2.162	0.171	0.056	0.419	0.242	0.219	0.035	0.038	**Gradient [dB/dB]**
	16.039	16.017	16.093	16.007	15.998	0.654	0.646	0.645	0.637	0.637	**Value [dB]**
OPTIMUM	*15.999*					*0.636*					**[dB]**
DOWN	15.961	15.983	15.906	15.993	16.002	0.641	0.637	0.670	0.644	0.650	**Value [dB]**
	0.893	0.397	2.143	0.169	0.056	0.116	0.028	0.772	0.179	0.318	**Gradient [dB/dB]**

Table 4.16: Overview of the perturbation around the optimum solution - target gain = 16 dB, C band, Variation = 1%.

Collected data are highly in agreement with the ones obtained in the previous analysis. In particular, sensitivity evaluations show that the gradient does not change significantly even increasing the entity of the variation applied from 1% to 10%. This property is remarkable because also in this case it is possible to linearize the function on a single dimension in the minimum working point and to use a single scalar number to describe performance modifications due to a single parameter variation.

Var = 5%	Average On-Off Gain					Ripple On-Off Gain					
	pp1	**pp2**	**pp3**	**pp4**	**pp5**	**pp1**	**pp2**	**pp3**	**pp4**	**pp5**	
	0.920	0.408	2.200	0.174	0.056	0.431	0.251	0.280	0.035	0.039	**Gradient [dB/dB]**
UP	16.195	16.087	16.467	16.037	15.989	0.727	0.689	0.695	0.643	0.644	**Value [dB]**
OPTIMUM	*15.999*					*0.636*					**[dB]**
	15.805	15.913	15.531	15.963	16.013	0.662	0.642	0.806	0.676	0.706	**Value [dB]**
DOWN	0.876	0.389	2.103	0.166	0.056	0.116	0.028	0.764	0.179	0.317	**Gradient [dB/dB]**

Table 4.17: Overview of the perturbation around the optimum solution - target gain = 16 dB, C band, Variation = 5%.

Var = 10%	Average On-Off Gain					Ripple On-Off Gain					
	pp1	**pp2**	**pp3**	**pp4**	**pp5**	**pp1**	**pp2**	**pp3**	**pp4**	**pp5**	
	0.940	0.418	2.247	0.178	0.056	0.435	0.257	0.310	0.036	0.138	**Gradient [dB/dB]**
UP	16.389	16.173	16.930	16.074	15.977	0.816	0.742	0.764	0.651	0.693	**Value [dB]**
OPTIMUM	*15.999*					*0.636*					**[dB]**
	15.609	15.827	15.061	15.926	16.026	0.816	0.742	0.764	0.651	0.693	**Value [dB]**
DOWN	0.854	0.379	2.053	0.162	0.056	0.111	0.076	0.749	0.175	0.311	**Gradient [dB/dB]**

Table 4.18: Overview of the perturbation around the optimum solution - target gain = 16 dB, C band, Variation = 10%.

Considering the on-off average gain, sensitivities are also symmetric with respect to the perturbation sign. This is not true for the on-off gain ripple because its value is related to maximum height of the on-off gain profile and it changes differently if the perturbation increases or decreases the pump power. This is related mainly to the interaction among pumps and spectrum which is described by the Raman efficiency curve. For the on-off average gain, the point is a little bit different because it is an average performance parameter and so the sign of the perturbation does not influence the gradient entity.
With respect to the previous case, only gradients of pumps placed at higher frequency (pumps 1, 2 and 3) increase. On the contrary gradients of pumps placed at lower frequency (pumps 4 and 5) seem to not vary sensibly with the increment of the on-off average gain target. It could be related to their position in frequency with respect to C band, because the peak of the Raman efficiency curve is located far from the band center. So, for this spectrum grid, sensitivities of pumps at lower frequencies are independent from the on-off average gain target.

4.5 Optimization in a multi-band scenario - 5 Raman pumps

After having studied the Raman amplification along a single fiber span on C band spectrum under a considerable quantity of cases, the focus moves to the optimization and the analysis of the Raman amplification in a C+L band scenario.

This kind of investigation is made in order to make some comparison between C band and C+L optimizations and to observe how performance parameters change modifying the transmitted input spectrum, which is one of the most important goal of the thesis activity.

The description of the scenario to optimize is reported in the following:

- Fiber link length $L_{span} = 120\,km$;
- C+L band grid (192 channels);
- Input power per channel $P_s = -10\,dBm$;
- 5 counter-propagating Raman pumps;
- Set of Raman pumps' wavelengths (fixed):
  - 1424 nm
  - 1438 nm
  - 1457 nm
  - 1470 nm
  - 1495 nm
- **5 variables problem**:
  - **Bounds on pumps powers**: $500\,mW \geq P_{p,i} \geq 0, \quad i = 1, ..., 5$
  - **Constraint on maximum total pumps power**: $\sum_{i=1}^{5} P_{p,i} = 1.2\,W$
  - **Object function**: $f(x) = \Delta G_{OO} + \mid \overline{G_{OO}} - \overline{G_{OO,target}} \mid$, with $\overline{G_{OO,target}} = 16\,dB$

As usual, in order to inspect the shape of the solution space, more than one optimization has been performed starting from different sets of initial values. In table 4.19 are reported the sets of initial input values.

Initial values				
Power pump 1 [mW]	**Power pump 2 [mW]**	**Power pump 3 [mW]**	**Power pump 4 [mW]**	**Power pump 5 [mW]**
50	50	50	50	50
100	100	100	100	100
150	150	150	150	150
200	200	200	200	200

Table 4.19: Sets of initial values for optimization, 5 Raman pumps, C+L band.

From each optimization final optimized configurations of pumps input powers are obtained. Their values are reported in table 4.20.
In this case, the prospective seems to be completely different from those shown in the previous sections.
As first observation, it is clear the fact that for each set of initial values the optimizer converges on a different optimum solution as before. Then, the entities of the

Final input configurations				
Power pump 1 [mW]	**Power pump 2 [mW]**	**Power pump 3 [mW]**	**Power pump 4 [mW]**	**Power pump 5 [mW]**
386	282	154	38	149
239	343	216	5e-20	184
309	320	204	2e-4	165
396	254	208	4e-13	154

Table 4.20: Sets of optimized input configurations, 5 Raman pumps, C+L band.

optimized input powers are in general much higher with respect to the equivalent C band optimum. The two cases do not share any similarity comparing optimized configurations. It is particularly curious the power value of the pump 4 which has 1470 nm of wavelength. From a mathematical point of view, the optimizer does not set this value to zero. On the other hand, from a practical point of view, it is not possible to handle the Raman pump power with a sensibility beyond the order of units of milliwatts. This is related to the aim of pump 4. It introduces just a very small power inside the fiber but along the first kilometers of fiber (starting from the end of the line), due to the Raman interaction among pumps, pumps at higher frequencies undergo the pump-pump depletion and they transfer power to the pump at 1470 nm that increases its power. In turn, the the pumping effect of the pump 4 is reflected on the spectrum. In this case, it is said that the pump is used as seed, in order to amplify the spectrum in a certain frequency portion exploiting the power introduces by Raman pumps placed at higher frequency. The same result cannot be possible if, for instance, the pump 4 is turned off, but at that frequency an amount of power, even small, has to be present.

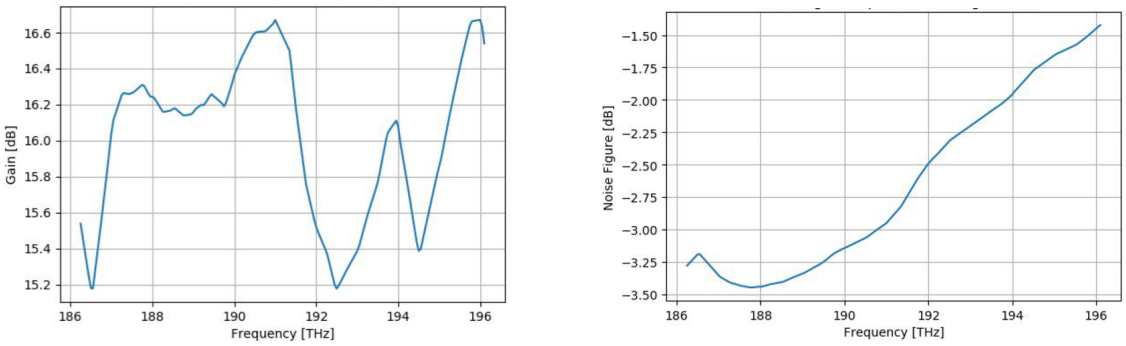

Figure 4.14: Optimization - gain and noise figure profiles, 5 Raman pumps, C+L band, target gain = 16 dB - scenario 1.

In figures 4.14, 4.15, 4.16 and 4.17 Raman on-off gain and noise figure profiles are reported for each optimization performed.
On-off gain profiles have an evident twisty shape linked to the Raman efficiency curve and to the position in frequency of the pumps. In every profile, peaks show the frequency range in which a certain pump has its maximum interaction with the spectrum. In particular, it is recognizable the peak caused by the pump at 1470 nm, which is the most important. Translating the pump wavelength in frequency, it is possible to determine analytically the peak position adding to the found pump frequency the frequency for which there is the strongest Raman interaction among

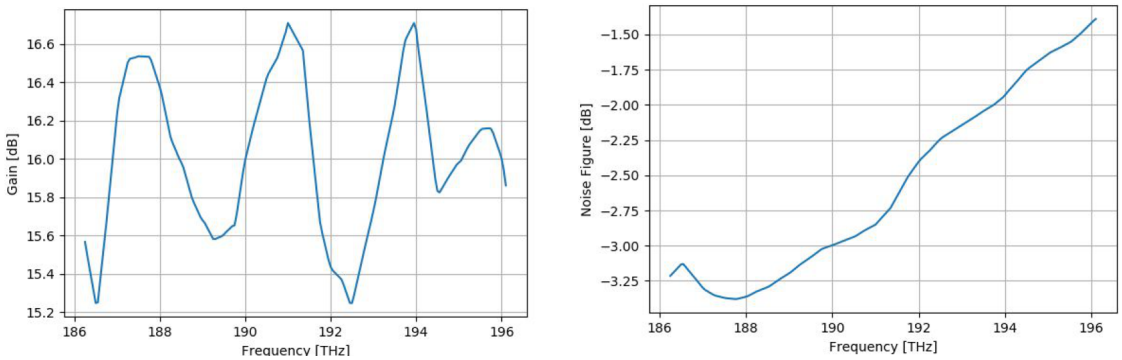

Figure 4.15: Optimization - gain and noise figure profiles, 5 Raman pumps, C+L band, target gain = 16 dB - scenario 2.

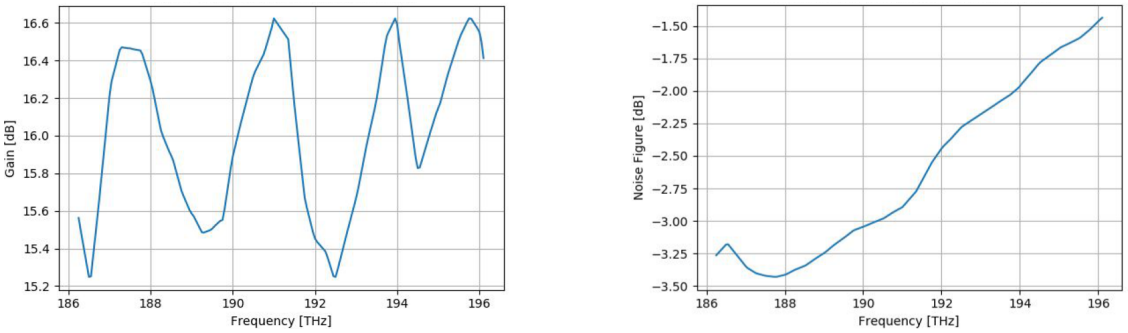

Figure 4.16: Optimization - gain and noise figure profiles, 5 Raman pumps, C+L band, target gain = 16 dB - scenario 3.

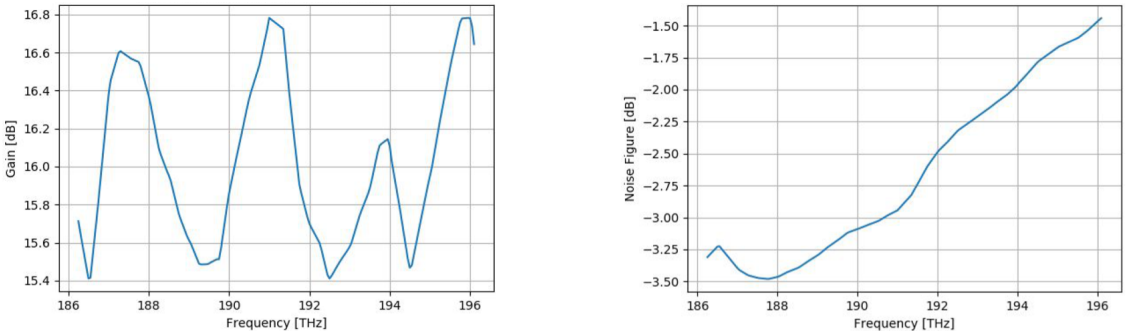

Figure 4.17: Optimization - gain and noise figure profiles, 5 Raman pumps, C+L band, target gain = 16 dB - scenario 4.

signal and pump: about 13 THz. This value resolves around 191 THz that is effectively the position of the peak in each on-off gain graph obtained.

In table 4.21 relative metrics of each optimum evaluated are reported.

The on-off average gain target is fully reached in any case. On the other hand, on-off gain ripple values are sensibly higher than those of the C band case. The optimizer has found optimum configurations that produce ripples with difference of more than 0.1 dB among them. In the previous case, each C band optimization presents on-off gain ripples that are quite similar. This means that the solution space has a shape that is strongly warped, so much that when a local minimum is

Metrics		
$\overline{G_{OO}}$ [dB]	ΔG_{OO} [dB]	**Function minimum [dB]**
15.999	1.494	1.494
15.999	1.462	1.462
15.999	1.375	1.375
16.000	1.371	1.371

Table 4.21: Metrics of optimized input configurations, 5 Raman pumps, C+L band.

reached, the optimizer is not able to pass towards the global minimum.

From the study of the Raman amplification optimization in the C+L band case, it is remarkable the fact that the scenario under analysis becomes more complex. In particular, the doubling of the input spectrum brings to a reduction of the performance in terms of on-off gain ripple for optimized Raman pumps input configurations, even if obtained values are quite satisfactory with respect to standards.
Analysing the behaviour of the optimizer under development, up to this point, it works fine for the problem under investigation formulated according the last objective function 3.4.

4.5.1 Input powers sensitivity evaluation

In order to evaluate the stability of system with respect to possible inputs variations, sensitivities of pumps input powers are evaluated around the optimum solution in this new C+L band case.

Also for this analysis, the perturbation is applied in percentage with respect to the pump input power entity and the optimized solution with the lowest function minimum is chosen for the investigation. For sake of clarity, the used optimum configuration of pumps is reported in the following:

- 1425 nm - $P_{p1,opt} = 396$ mW
- 1438 nm - $P_{p2,opt} = 254$ mW
- 1457 nm - $P_{p3,opt} = 208$ mW
- 1470 nm - $P_{p4,opt} =$ 4e-13 mW
- 1495 nm - $P_{p5,opt} = 154$ mW

In tables 4.22, 4.23 and 4.24 are reported information related to gradient computations and performance modifications. Comparing gradients of same pumps among tables for different applied variations, it is now appreciable the fact that values are not so similar, and so the multi-dimensional space is no more linear along a single dimension as in the previous cases.
Observing gradient values of on-off average gain, it is possible to say that for many

Var = 1%	Average On-Off Gain					Ripple On-Off Gain					
	pp1	**pp2**	**pp3**	**pp4**	**pp5**	**pp1**	**pp2**	**pp3**	**pp4**	**pp5**	
	1.376	0.949	0.951	6e-12	0.928	0.296	0.253	0.799	9e-12	0.567	**Gradient [dB/dB]**
UP	16.060	16.041	16.041	16.000	16.040	1.384	1.382	1.405	1.371	1.395	**Value [dB]**
OPTIMUM	*16.000*					*1.371*					**[dB]**
	15.941	15.959	15.959	16.000	15.960	1.398	1.374	1.398	1.371	1.469	**Value [dB]**
DOWN	1.363	0.939	0.942	8e-14	0.921	0.626	0.075	0.612	2e-11	2.252	**Gradient [dB/dB]**

Table 4.22: Overview of the perturbation around the optimum solution - target gain = 16 dB, C+L band, Variation = 1%.

Var = 5%	Average On-Off Gain					Ripple On-Off Gain					
	pp1	**pp2**	**pp3**	**pp4**	**pp5**	**pp1**	**pp2**	**pp3**	**pp4**	**pp5**	
	1.407	0.968	0.969	2e-12	0.941	0.344	0.260	0.812	1e-12	0.966	**Gradient [dB/dB]**
UP	16.298	16.205	16.205	16.000	16.199	1.384	1.426	1.543	1.371	1.575	**Value [dB]**
OPTIMUM	*16.000*					*1.371*					**[dB]**
	15.703	15.795	15.794	16.000	15.798	1.398	1.387	1.506	1.371	1.869	**Value [dB]**
DOWN	1.332	0.920	0.923	1e-12	0.907	0.617	0.071	0.607	2e-12	2.238	**Gradient [dB/dB]**

Table 4.23: Overview of the perturbation around the optimum solution - target gain = 16 dB, C+L band, Variation = 5%.

Var = 10%	Average On-Off Gain					Ripple On-Off Gain					
	pp1	**pp2**	**pp3**	**pp4**	**pp5**	**pp1**	**pp2**	**pp3**	**pp4**	**pp5**	
	1.443	0.991	0.991	5e-13	0.958	0.617	0.271	0.816	7e-13	0.518	**Gradient [dB/dB]**
UP	16.597	16.410	16.410	16.000	16.396	1.616	1.482	1.713	1.371	1.999	**Value [dB]**
OPTIMUM	*16.000*					*1.371*					**[dB]**
	15.407	15.590	15.588	16.000	15.593	1.643	1.463	1.644	1.371	2.387	**Value [dB]**
DOWN	1.295	0.895	0.900	3e-14	0.889	0.594	0.142	0.597	1e-12	2.220	**Gradient [dB/dB]**

Table 4.24: Overview of the perturbation around the optimum solution - target gain = 16 dB, C+L band, Variation = 10%.

pumps the property of symmetry with respect to the sign of variation is lost for high percentages.
About gradients entities of pump 4, they are so low because basically the response of the whole system depends on pumps power located at higher frequency. The overall amplification is determined by the pumping effect of pumps 1, 2 and 3 on pump 4, that in its turn transfers power to pump 5 and to the spectrum.

In general, the C+L band system is more susceptible to perturbations of pumps input powers cause to the enlargement of the band, which becomes more difficult to control with the same number of pumps. This is particularly true observing on-off average gain gradients of pump 1 and on-off gain ripple gradients.
In base on this consideration and the previous analysis on sensitivities, it is possible

to affirm that the function which describes the solution space is nonlinear close to the optimum solution and it is no more possible to define a single scalar parameter which uniquely defines the entity of the system performance given a certain perturbation in the optimum working point.

4.5.2 Wavelengths sensitivity evaluation

The analysis of the stability of the Raman optimum configuration continues evaluating performance modifications with respect to possible variations of Raman pumps wavelengths.
This new study has been made cause of the reduction of performance passing from the C band scenario to the C+L band one and the criticalities observed during the examination of pumps input power sensitivities. From this, it has been possible to understand if a certain pump has to be strictly stable in its frequency position in order to not degrade performance in not acceptable way.

Var = 1 nm	Average On-Off Gain					Ripple On-Off Gain					
	λp1	**λp2**	**λp3**	**λp4**	**λp5**	**λp1**	**λp2**	**λp3**	**λp4**	**λp5**	
UP	0.015	0.041	0.053	4e-14	0.089	0.373	0.117	0.330	4e-13	0.215	**Gradient [dB/dB]**
	16.014	16.041	16.053	16.000	15.910	1.744	1.488	1.700	1.371	1.586	**Value [dB]**
OPTIMUM	*16.000*					*1.371*					**[dB]**
DOWN	15.979	15.963	15.951	16.000	16.086	1.441	1.663	1.542	1.371	1.695	**Value [dB]**
	0.021	0.037	0.049	3e-13	0.086	0.070	0.292	0.171	2e-13	0.324	**Gradient [dB/dB]**

Table 4.25: Overview of the perturbation around the optimum solution - target gain = 16 dB, C+L band, Variation = 1 nm.

Var = 2 nm	Average On-Off Gain					Ripple On-Off Gain					
	λp1	**λp2**	**λp3**	**λp4**	**λp5**	**λp1**	**λp2**	**λp3**	**λp4**	**λp5**	
UP	0.015	0.041	0.054	4e-14	0.090	0.371	0.114	0.348	2e-13	0.300	**Gradient [dB/dB]**
	16.029	16.083	16.108	16.000	15.820	2.113	1.599	2.068	1.371	1.971	**Value [dB]**
OPTIMUM	*16.000*					*1.371*					**[dB]**
DOWN	15.959	15.928	15.903	16.000	16.169	1.616	1.963	1.721	1.371	2.024	**Value [dB]**
	0.020	0.036	0.048	1e-13	0.084	0.122	0.296	0.175	4e-13	0.327	**Gradient [dB/dB]**

Table 4.26: Overview of the perturbation around the optimum solution - target gain = 16 dB, C+L band, Variation = 2 nm.

The computation of wavelength sensitivities is carried out according to absolute variations. This approach brings to have a kind of results that is more readable from a practical point of view. it is related to the fact that Raman pumps are LASERs in essence and their wavelength is taken under control by a grating at the output of the device. Generally, it allows to maintain the wavelength in a range of

Var = 3 nm	Average On-Off Gain					Ripple On-Off Gain					
	λp1	**λp2**	**λp3**	**λp4**	**λp5**	**λp1**	**λp2**	**λp3**	**λp4**	**λp5**	
UP	0.015	0.041	0.053	6e-14	0.090	0.364	0.113	0.351	1e-13	0.334	**Gradient [dB/dB]**
	16.045	16.125	16.159	16.000	15.730	2.464	1.709	2.423	1.371	2.372	**Value [dB]**
OPTIMUM	*16.000*					*1.371*					**[dB]**
DOWN	15.942	15.893	15.860	16.000	16.235	1.845	2.269	1.954	1.371	2.816	**Value [dB]**
	0.019	0.036	0.047	1e-13	0.078	0.158	0.299	0.195	5e-14	0.482	**Gradient [dB/dB]**

Table 4.27: Overview of the perturbation around the optimum solution - target gain = 16 dB, C+L band, Variation = 3 nm.

a few nanometers.
For this reason, performance variations are easily evaluated knowing the entity of the variation in absolute value and not relative.

In tables 4.25, 4.26 and 4.27 information on gradient computation with respect to wavelength variation and the relative modification of performances are reported. In this case, many features already observed in the previous analysis on C band input power sensitivity.
First of all, considering gradients of the same wavelength with the increasing of the applied variation, sensitivities are almost the same. This is true both for on-off average gain and on-off gain ripple. The only parameter that does not respect this behaviour is the sensitivity of the on-off gain ripple with respect to the wavelength variation of pump 5. This one is used to manage the peak of the on-off gain profile placed at the bottom of the L band and so it is understandable the increasing of the gradient value with the further shifting of the pump wavelength towards higher values.
Then, observing the on-off average gain gradients, they are also symmetric with respect to the sign of the perturbation. In general, this property is not respected for on-off gain ripple gradient because the perturbation is now applied to the frequency position of the Raman pump and this tends to enhance the twisting of the on-off gain curve. Instead, the on-off average gain is a mean of the profile values, and so the sensitivity does not depend from sign of the perturbation.
In general, especially for the reason just expressed, average sensitivities are more moderate than ripple ones, in view of the fact that the frequency shift of pumps determines a further modification on the profile which reduces the degree of flatness of the curve and degrades on-off gain ripple performance.

From the last analysis, it has been understood that the C+L scenario described can be linearized for small variations of wavelength around the optimum solution. This property is very important from a practical point of view in order to characterize performance deviations of the system through the sensitivity parameter.
Furthermore, the frequency position of pump at 1495 nm (lowest frequency) results to be most important in terms of performance degradation with this configuration. So it has to be more stable than the others in order to not increase the maximum on-off gain ripple.

4.6 Adding Raman pumps' wavelengths as optimization variables

After having performed an exhaustive analysis on the C+L scenario, the question has been moved to the possibility of refining the optimum solution performing a new optimization that takes into account both pumps input power and wavelength. Tuning with finely every parameter, the target is to reduce the on-off gain ripple in C+L scenario maintaining the on-off average gain stable.

To reach this purpose, the optimization problem has been enlarged defining as input variables to optimize both input powers and wavelength of the Raman pumps, passing from 5 variables to 10.
Starting from the previous optimum solution, bounds of each input power variable are imposed in a smaller range in order to carry out just an improvement, avoiding to increasing in excessive way the optimization time. Instead, wavelengths bounds are kept into the range of ± 3 nm.

The description of the scenario to optimize is reported in the following:

- Fiber link length $L_{span} = 120\,km$;
- C+L band grid (192 channels);
- Input power per channel $P_s = -10\,dBm$;
- 5 counter-propagating Raman pumps;
- Set of initial Raman pumps' input powers:
  - $P_{p1,0} = 396$ mW
  - $P_{p2,0} = 254$ mW
  - $P_{p3,0} = 208$ mW
  - $P_{p4,0} = 4\text{e-}13$ mW
  - $P_{p5,0} = 154$ mW
- Set of initial Raman pumps' wavelengths:
  - $\lambda_{p1,0} = 1424$ nm
  - $\lambda_{p2,0} = 1438$ nm
  - $\lambda_{p3,0} = 1457$ nm
  - $\lambda_{p4,0} = 1470$ nm
  - $\lambda_{p1,0} = 1495$ nm
- **10 variables problem**:
  - **Bounds on pumps powers**: $(P_{pi,0} + 25\,mW) \geq P_{pi} \geq (P_{pi,0} - 25\,mW)$, $i = 1, ..., 5$
  - **Bounds on pumps wavelengths**: $(\lambda_{pi,0} + 3\,nm) \geq \lambda_{pi} \geq (\lambda_{pi,0} - 3\,nm)$, $i = 1, ..., 5$

- **Constraint on maximum total pumps power**: $\sum_{i=1}^{5} P_{pi} = 1.2\,W$
- **Object function**: $f(x) = \Delta G_{OO} + \mid \overline{G_{OO}} - \overline{G_{OO,target}} \mid$, with $\overline{G_{OO,target}} = 16\,dB$

The optimization is performed twice introducing each time a different input spectrum.
In the first case, the standard C+L band pattern has been used.
In the second one, in order to perform a reduction of the optimization time, the granularity of the initial input pattern has been decreased joining and making the average of groups of 4 channels and summing their input powers in the following way:

$$f_{s,k}^{new} = \frac{1}{4} \sum_{i=1+4*(k-1)}^{4+4*(k-1)} f_{s,i} \qquad with \quad k = 1, 2, ..., \frac{N_{ch}}{4}$$

$$P_s(f_{s,k}^{new}) = \sum_{i=1+4*(k-1)}^{4+4*(k-1)} P_s(f_{s,i}) \qquad with \quad k = 1, 2, ..., \frac{N_{ch}}{4}$$

where P_s are signal input powers in linear units.

Using this more compact equivalent spectrum, the set of ordinary differential equations is lightened because the number of channels passes from 192 to 48 nominal channels and consequently the mathematical system is faster to solve.

In tables 4.28, 4.29, 4.30 and 4.31 are reported the final configurations of optimized pumps input powers and wavelength for both standard C+L spectrum and reduced C+L spectrum.

Final input configuration (complete spectrum, 192 nominal channels)				
Power pump 1 [mW]	**Power pump 2 [mW]**	**Power pump 3 [mW]**	**Power pump 4 [mW]**	**Power pump 5 [mW]**
386.437	263.588	183.000	14.868	157.905

Table 4.28: Set of refined input parameters around optimum, 5 Raman pumps, C+L band, complete C+L spectrum - pumps input power.

Final input configuration (complete spectrum, 192 nominal channels)				
λ pump 1 [nm]	**λ pump 2 [nm]**	**λ pump 3 [nm]**	**λ pump 4 [nm]**	**λ pump 5 [nm]**
1423.937	1438.821	1456.716	1469.839	1494.996

Table 4.29: Set of refined input parameters around optimum, 5 Raman pumps, C+L band, complete C+L spectrum - pumps wavelength.

From the obtained optimized configurations, it is possible to notice that in both cases input powers undergo a refinement that is rather similar; pumps 1 and 2 differ more that others in terms of absolute values.
Comparing wavelengths, pumps 2 and 4 slightly diverge, while the others maintain almost values close to the initial ones.

Final input configuration (reduced spectrum, 48 nominal channels)				
Power pump 1 [mW]	**Power pump 2 [mW]**	**Power pump 3 [mW]**	**Power pump 4 [mW]**	**Power pump 5 [mW]**
371.359	276.835	187.326	0.440	163.343

Table 4.30: Set of refined input parameters around optimum, 5 Raman pumps, C+L band, reduced C+L spectrum - pumps input power.

Final input configuration (reduced spectrum, 48 nominal channels)				
λ pump 1 [nm]	**λ pump 2 [nm]**	**λ pump 3 [nm]**	**λ pump 4 [nm]**	**λ pump 5 [nm]**
1423.509	1439.758	1457.191	1468.323	1494.329

Table 4.31: Set of refined input parameters around optimum, 5 Raman pumps, C+L band, reduced C+L spectrum - pumps wavelength.

In general, the optimization of input powers is led by the placement of Raman pumps in frequency, and so the difference in final configurations of pumps input powers is due to this reason.

In figure 4.18, the on-off gain and noise figure profiles of the optimized scenario with the complete input pattern are reported. The relative metrics is present in table 4.32.

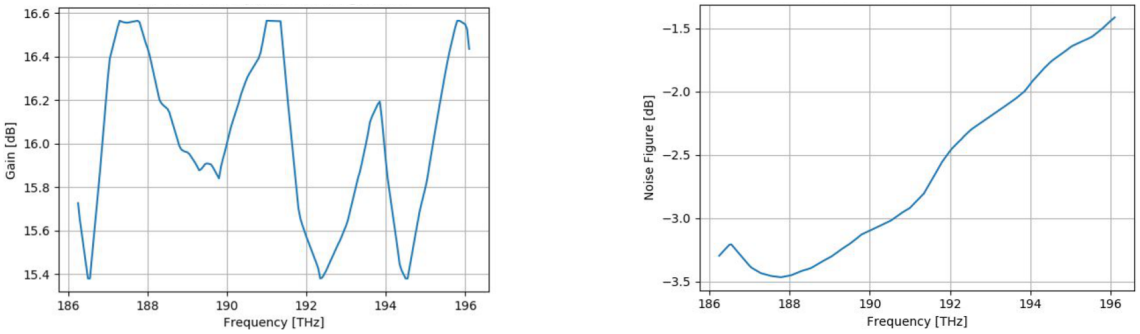

Figure 4.18: Optimization - gain and noise figure profiles, complete C+L spectrum.

Metrics (complete spectrum)			
$\overline{G_{OO}}$ [dB]	ΔG_{OO} [dB]	**Function Minimum [dB]**	**Time [days]**
16.000	1.186	1.186	5.3

Table 4.32: Metrics of refined input parameters around optimum, 5 Raman pumps, C+L band, complete spectrum.

On the other hand, in figure 4.19, the on-off gain and noise figure profiles of the optimized scenario with the reduced input pattern are reported. The relative metrics is available in table 4.33.

Firstly, observing the on-off average gain, it is always reached in both cases. Being

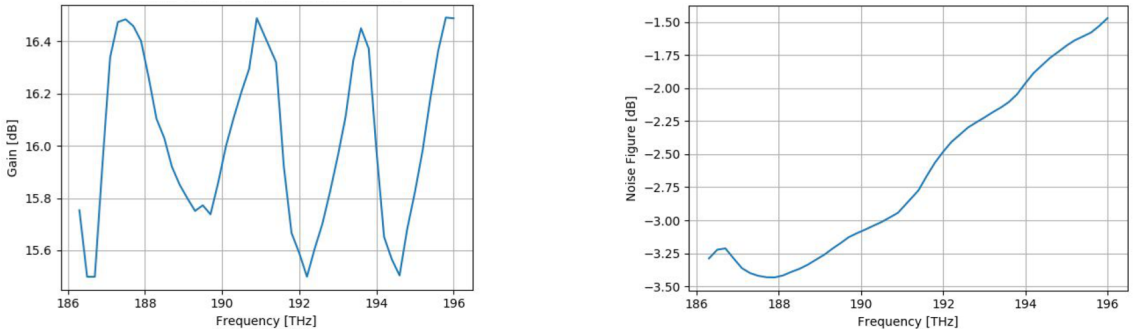

Figure 4.19: Optimization - gain and noise figure profiles, reduced C+L spectrum.

Metrics (reduced spectrum)			
$\overline{G_{OO}}$ **[dB]**	ΔG_{OO} **[dB]**	**Function Minimum [dB]**	**Time [hours]**
16.002	0.992	0.994	7.2

Table 4.33: Metrics of refined input parameters around optimum, 5 Raman pumps, C+L band, reduced C+L spectrum.

the last optimization a refinement of the previous one, it is clear that the the initial working point has been already near to the on-off average gain target.
Then, analysing the on-off gain ripples, they have been refined effectively having a reduction of about 0.2 dB for the case with complete C+L input spectrum and of 0.4 dB in the case of reduced C+L input spectrum with respect to the previous optimization.
The loss of information related to the lowering of the granularity does not allowed to achieve the same result in terms of final optimized values and metrics. On the other hand, even if the two input configurations differ one from the other, the overall behaviour of on-off gain profiles is preserved.
Furthermore, the time spent for a single optimization in the case of reduced input pattern has an improvement of about 94% with respect to the complete one.

Chapter 5

Conclusion

In the present work, an optimization tool has been developed to make efficient and suitable the design of Raman amplifiers, starting from a physical layer description of an optical fiber link.
The optimization framework is able to determine parameters of Raman pumps - as optical input power and wavelength - in base on requests of the design with the maximum performance in terms of flatness of the on-off gain profile.
The investigation has been carried out before on C band scenarios, analysing the shape of the solution space of interest and so evaluating the stability of the system throughout the application of small perturbations around the optimum solution.
Then, the same analysis has been made during the study of scenarios in C+L band.
In order to improve the obtained result in terms of performance, the optimization problem has been enlarged refining the complete set of Raman pumps input powers and wavelengths.

The actual optimization tool works fine for the proposed problem. In particular, with the last adopted formulation the optimizer is able to determine with high precision a Raman pumps input configuration with a certain gain target minimizing the ripple. A successful outcome is reach both in single band and in multi-band scenarios.
The analysis around the optimum working point has been useful to understand the phenomenon and to plan the future development of the activity. From the studied cases, two important results have been observed from a mathematical point of view.
The first one is related to the convexity of the solution space. It seems to have a single well defined global minimum for C band scenarios with moderate on-off average gain (around 10 dB or below). For C+L band scenarios or for higher values of on-off average gain, the optimizer shows that there is more than one input configuration which clips the on-off average gain target. Once the target is reached, the final solution varies cause to different minimization in base on the local minimum of the solution space.
The second important mathematical result is that around the optimum solution it is possible to linearize the multi-dimensional space according to any single dimension for small perturbation both for Raman pumps input powers and wavelengths. This is extremely significant also from a practical point of view because it is faster to make predictions on performance modifications due to input parameters perturbations.

In the prospective of further improvements, the object function can be reformulated in order to make the solution space convex. Currently, the on-off average gain is a parameter that gives a perception of the performance behaviour in the overall frequency span. One option could be to define different terms of on-off average gain in the objective function related to different frequency slices. In this way, the higher accuracy with which the on-off average gain is locally defined in the frequency range could bring to the uniqueness of the optimum solution.
Another chance could be the adoption of a new metrics that takes into account average gain and ripple values refereed to C and L bands separately in the case of C+L scenarios, as in the analysis carried out with the brute force strategy.
Furthermore, software improvements are strongly needed in order to speed up optimization time. Now, optimization on 5 variables problems spent on average hours for C band scenario and tenths of hours for C+L band scenarios, and complete optimizations on 10 variables problems spent time of the order of some days.

This work provides also a significant outlet for lab validations. In particular, the whole framework has to be test comparing analytical data with experimental ones, evaluating the quality of the model under appropriate conditions and dealing with the sensibility of measure instrumentation.
In addition to this, in order to fill the sake of knowledge related to the incomplete mirroring of the analytical model in the real world, machine-learning techniques could be implemented, improving also the optimization time.

Bibliography

[1] Zh I Alferov et al. "Investigation of the influence of the AlAs-GaAs heterostructure parameters on the laser threshold current and the realization of continuous emission at room temperature". In: *Sov. Phys. Semicond* 4.7 (1971), pp. 1573–1575.

[2] Jake Bromage. "Raman amplification for fiber communications systems". In: *Journal of Lightwave Technology* 22.2 (2004), p. 79.

[3] Andrea Carena, Vittorio Curri, and Pierluigi Poggiolini. "On the optimization of hybrid Raman/erbium-doped fiber amplifiers". In: *IEEE Photonics Technology Letters* 13.11 (2001), pp. 1170–1172.

[4] Kin S Chiang. "Intermodal dispersion in two-core optical fibers". In: *Optics letters* 20.9 (1995), pp. 997–999.

[5] VNI Cisco. "Cisco visual networking index: Forecast and trends, 2017–2022". In: *White Paper* 1.3 (2018).

[6] SciPy community. *SciPy*. 2018-2019. URL: `https://docs.scipy.org/doc/scipy/reference/index.html`.

[7] Kiyoshi Fukuchi et al. "10.92-Tb/s (273 x 40-Gb/s) triple-band/ultra-dense WDM optical-repeatered transmission experiment". In: *Optical Fiber Communication Conference*. Optical Society of America. 2001, PD24.

[8] PB Hansen et al. "Capacity upgrades of transmission systems by Raman amplification". In: *IEEE Photonics Technology Letters* 9.2 (1997), pp. 262–264.

[9] I Hayashi et al. "Junction lasers which operate continuously at room temperature". In: *Applied Physics Letters* 17.6 (1970), pp. 109–111.

[10] Mohammed N Islam. "Raman amplifiers for telecommunications". In: *IEEE Journal of selected topics in Quantum Electronics* 8.1 (2002), pp. 548–559.

[11] KC Kao and George A Hockham. "Dielectric-fibre surface waveguides for optical frequencies". In: *Proceedings of the Institution of Electrical Engineers*. Vol. 113. 4. IET. 1966, pp. 1151–1158.

[12] Simon Kemp. *Digital 2019: Global Digital Overview*. 2019. URL: `https://datareportal.com/reports/digital-2019-global-digital-overview`.

[13] Guifang Li. "Recent advances in coherent optical communication". In: *Advances in optics and photonics* 1.2 (2009), pp. 279–307.

[14] Lynn E Nelson et al. "High-capacity, Raman-amplified long-haul transmission and the impact of optical fiber properties". In: *Optical Transmission Systems and Equipment for WDM Networking II*. Vol. 5247. International Society for Optics and Photonics. 2003, pp. 26–39.

[15] A Polman et al. “Optical doping of waveguide materials by MeV Er implantation”. In: *Journal of applied physics* 70.8 (1991), pp. 3778–3784.

[16] Telecom Infra Project. *Telecom Infra Project*. 2019. URL: `https://telecominfraproject.com/`.

[17] Chandrasekhara Venkata Raman and Kariamanikkam Srinivasa Krishnan. “A new type of secondary radiation”. In: *Nature* 121.3048 (1928), p. 501.

[18] Karsten Rottwitt and Andrew J Stentz. “Raman amplification in lightwave communication systems”. In: *Optical Fiber Telecommunications IV-A*. 5. Elsevier, 2002, pp. 213–257.

[19] Yoshinori Yamamoto, Masaaki Hirano, and Takashi Sasaki. “A new class of optical fiber to support large capacity transmission”. In: *2011 Optical Fiber Communication Conference and Exposition and the National Fiber Optic Engineers Conference*. IEEE. 2011, pp. 1–3.